Gravitational waves from binary black hole mergers in active galactic nuclei

Matthias Gröbner

Supervised by
Wako Ishibashi
Shubhanshu Tiwari

in the group of
Philippe Jetzer

at the
Universität Zürich

Zürich, September 2019

Acknowledgement

Contents

1 Introduction

1.1 Metaphysical introduction

The currently established theory of gravity is based on the idea that "curved spacetime tells matter how to move" and that "matter tells spacetime how to curve". In fact, the device of spacetime has been so successful that it has already been built into the languages we speak. However, it is not always realized how abstract the information is that theoretical physics gives. On top of that, all that physics gives us are certain functional equations that allow us to organize and structure events *we* experience. Physics is silent about whether our abstract notions appearing in the equations (like electrical fields, spacetime or entangled spinor quantum fields) represent an underlying "physical reality". In fact, it would be a mistake to introduce our abstract concepts into the world and reify them. In Niels Bohr's words: "It is wrong to think that the task of physics is to find out how nature is. Physics concerns what we can say about nature." Understanding the world and knowing what "really happens" is a much higher inspiration than understanding theories about the world, and physics and science can only do the latter. One could go further and even assert that "*my* physics concern what *I* can say about *my* world." Such positions may be purely motivated by philosophy, but thinking about quantum mechanics has also brought such positions to some physicists.

In this light, what do we mean when we say "spacetime", a word which lies at the foundations of the theory of general relativity? What is "spacetime"? In light of the above position we (or rather I) would answer: Time and space are modes by which we (or I) think, which we (or I) invented to organize events we (or I) experience; space and time are not conditions in which we (or I) live (apparently this is a quote even attributed to Einstein, but this seems unlikely since the content is hard to reconcile with his objections to quantum mechanics.) In any case, in this chapter I give a frightening abstract definition of a manifold. The abstractness of this first section is intended to remind myself that I should refrain from reifing mathematical or mental concepts into the world. What does it possibly mean that a locally ringed space locally isomorphic to $\mathbb{R}^4$ with its sheaf of differentiable functions (and endowed with more algebraic structure) "is really out there"? If one believes in Bourbaki's philosophy that everything in mathematics can be accommodated within set theory, the "ontology of spacetime (or quantum mechanics etc.)" is reduced to the "ontology of set theory". So, what meaning has the question: Is set theory "out there"?

In physics coordinates systems are used all the time. At the same time, especially in general relativity, it is acknowledged that local coordinates have no prominent role in the theory. Nevertheless, the usual construction of "spacetime", that is of manifolds with some extra structure, explicitly uses local coordinate charts; this can lead to overemphasize them and to conceptual confusion as well. A second purpose of this section is to provide an antidote to this by outlining a construction of "spacetime" where charts and atlases do not play any central role. This is conceptually satisfying, but it has to be admitted that this is a somewhat foundational issue and the adopted viewpoint is not much of a practical use in general relativity and even differential geometry.

1.2 Mathematical introduction

As advertised in the metaphysical introduction, we will in this section provide a formalization of a manifold in a non-coordinate fashion. We also make a note on principal bundles. The established notions are enough to then shed some light on the formulation of general relativity.

1.2.1 Sheaf-theoretic definition of a smooth manifold

One key insight of algebraic geometry is that we can understand spaces by understanding the functions on them; more precisely, we can understand a space by characterizing all functions on all open subsets of this space. This kind of information is encoded in the sheaf of functions on a space. We can so to speak reverse the engine and start *defining* basic geometric models by their sheaves. We can then built richer geometries by gluing together these basic objects in a way that is made precise by the notion of ringed spaces and morphisms between them. This framework is indispensable for algebraic geometry, but it can also be used to formalize the notion of a manifold. We will state the general definitions and afterwards apply them to the setting of differential geometry. A reference for this section is *e.g.* the Stacks Project [1].

Presheaves and Sheaves Roughly speaking, a presheaf is a way to assign data locally to open subsets of a topological space in such a way that it is compatible with restrictions. A sheaf is a presheaf for which it is possible to reassemble global information about a space from local data.

A presheaf of $\mathcal{C}$ on a topological space X is a contravariant functor $\mathcal{F} : \mathrm{Ouv}(X) \to \mathcal{C}$. The category $\mathrm{Ouv}(X)$ is the category whose objects are the open subsets of X and whose morphisms are inclusions. Usually $\mathcal{C}$ is the category of sets, rings, groups, ... The elements in $\mathcal{F}(U)$ are called the sections of $\mathcal{F}$ over U. Given $V \subseteq U$ in $\mathrm{Ouv}(X)$ and the inclusion map $f : V \to U$, the map $\mathcal{F}(f) : \mathcal{F}(U) \to \mathcal{F}(V)$ is denoted by res_V^U and is called the restriction map.

Given a topological space X, we can map an open set U to the set of smooth maps $U \to \mathbb{R}$. The set $C^\infty(U, \mathbb{R})$ has the structure of a ring, therefore we have a presheaf $\mathcal{C}_X^\infty$ of rings on X ("presheaf of smooth functions on X"). The restriction map restricts a smooth map $U \to \mathbb{R}$ to the open subspace $V \subseteq U$.

A presheaf $\mathcal{F}$ is a sheaf if given any open subset $U \subset X$ and an open cover $U = \bigcup_\alpha U_\alpha$, the two conditions are satisfied

1. if $s, t \in \mathcal{F}(U)$ are such that $s|_{U_\alpha} = t|_{U_\alpha}$ for all α, then $s = t$ in $\mathcal{F}(U)$,

2. if $s_\alpha \in \mathcal{F}(U_\alpha)$ is a collection of sections which agree when restricted to their intersections $U_\alpha \cap U_\beta$, then there is a $s \in \mathcal{F}(U)$ which restricts to each s_α on $U_\alpha \subseteq U$.

The presheaf of smooth functions is a sheaf. Indeed, in a somewhat obvious way we have:

1. Let $s, t : U \to \mathbb{R}$ and suppose that s and t agree on each open subset in a cover of U. We need to show that $s(x) = t(x)$ for all $x \in U$. Let $x \in U$, then $u \in U_i$ for some i. We then have $s(x) = s|_{U_i}(x) = t|_{U_i}(x) = t(x)$.

2. Let $U = \bigcup_i U_i$ and let s_i be sections which agree on their intersections. We can define a map $s : U \to \mathbb{R}$ by taking $x \in U$ and some U_i which contains x, and setting $s(x) = s_i(x)$. This is independent of the U_i chosen, because all s_i agree on intersections. The function s is smooth since all s_i are smooth and since smoothness of a function is a local property.

Let $\mathcal{F}$ and $\mathcal{G}$ be presheaves of $\mathcal{C}$ on X. A morphism of presheaves $\phi : \mathcal{F} \to \mathcal{G}$ is a family of morphisms in $\mathcal{C}$ $\phi_U : \mathcal{F}(U) \to \mathcal{G}(U)$ for each open $U \subset X$ such that given an inclusion $V \subseteq U$ we have the commutative diagram

$$
\begin{array}{ccc}
\mathcal{F}(U) & \xrightarrow{\phi_U} & \mathcal{G}(U) \\
\downarrow{\scriptstyle \mathrm{res}_V^U} & & \downarrow{\scriptstyle \mathrm{res}_V^U} \\
\mathcal{F}(V) & \xrightarrow{\phi_V} & \mathcal{G}(V).
\end{array}
$$

A morphism of sheaves is a morphism of the underlying presheaves. We also need a tool to study sheaves and presheaves locally. For any presheaf $\mathcal{F}$ and any point $x \in X$, we define the stalk $\mathcal{F}_x$ to be

$$
\mathcal{F}_x = \{(U, s) \mid x \in U, s \in \mathcal{F}(U)\}/\sim,
$$

where $(U, s) \sim (U', s')$ if and only if there exists $V \subset U \cap U'$ such that $s|_V = s'|_V$.

An element of the stalk $\mathcal{C}_{X,x}^\infty$ of $\mathcal{C}_X^\infty$ at x is thus a C^∞-function f whose domain contains x. A pair of such functions f, g determine the same element of the stalk if they agree in a neighbourhood of x. Such an equivalence class is called a germ of a C^∞-function at x and the stalk $\mathcal{C}_{X,x}^\infty$ is then the ring of germs of smooth functions at x. The stalk $\mathcal{C}_{X,x}^\infty$ is a local ring with maximal ideal $\mathfrak{m} = \{[(U, f)] \mid f(x) = 0\}$; this means that the ideal $\mathfrak{m}$ is the set of non-invertible elements in $\mathcal{C}_{X,x}^\infty$. Indeed, for the germ at x of a smooth function to be invertible in $\mathcal{C}_{X,x}^\infty$, it is necessary and sufficient that $f(x) \neq 0$, for this implies that $f(x) \neq 0$ in a neighbourhood of x.

Given a continuous map $f : X \to Y$ of topological spaces and a presheaf $\mathcal{F}$ on X, the pushforward $f_* \mathcal{F}$ is the presheaf on Y defined by $(f_* \mathcal{F})(V) = \mathcal{F}(f^{-1}(V))$ for $V \in \mathrm{Ouv}(Y)$. The pushforward $f_* \mathcal{F}$ of a sheaf $\mathcal{F}$ on X is a sheaf on Y.

Locally ringed spaces We will define a type of structure that lends itself well to construct spaces by gluing together different spaces along open sets.

A ringed space is a pair $(X, \mathcal{O}_X)$ consisting of a topological space and a sheaf of rings $\mathcal{O}_X$. A morphism of ringed spaces $(f, f^\sharp) : (X, \mathcal{O}_X) \to (Y, \mathcal{O}_Y)$ is a continuous map of topological spaces $f : X \to Y$ and a morphism of sheaves $f^\sharp : \mathcal{O}_Y \to f_* \mathcal{O}_X$. The map $f^\sharp$ is simply precomposition when working with ringed spaces whose sheaf is that of smooth functions. That is, to $f : X \to Y$ and $\varphi : V \to \mathbb{R} \in \mathcal{C}_Y^\infty$ there is associated the map $f^\sharp = \varphi \circ (f|_{f^{-1}(V)}) \in \mathcal{C}_X^\infty(f^{-1}(V))$.

We will impose a condition relating the geometry of X with the algebra of $\mathcal{O}_X$. One motivation for doing this really comes from algebraic geometry: The functor from the category of rings to the category of ringed spaces is not fully faithful: It is possible that there are maps between ringed spaces that are not

induced by maps of rings. We therefore want to impose a condition restricting the set of morphisms. We will see that ringed spaces with sheaves of differentiable functions naturally fall into this framework (but we will not prove that this notion provides the claimed linkage between geometry and algebra).

A locally ringed space is a ringed space $(X, \mathcal{O}_X)$ so that for all $x \in X$ the stalk $\mathcal{O}_{X,x}$ is a local ring. A morphism of locally ringed spaces $(f, f^\sharp) : (X, \mathcal{O}_X) \to (Y, \mathcal{O}_Y)$ is a morphism of ringed spaces such that for all $x \in X$ the map of local rings $f_x^\sharp : \mathcal{O}_{Y,f(x)} \to \mathcal{O}_{X,x}$ is a local ring morphism. A morphism of local rings $f : R \to S$ is called local if $f^{-1}(\mathfrak{m}_S) = \mathfrak{m}_R$.

We already know that the stalk $\mathcal{C}_{X,x}^\infty$ is a local ring, therefore the pair $(X, \mathcal{C}_X^\infty)$ is a locally ringed space. Given two such pairs $(X, \mathcal{C}_X^\infty)$ and $(Y, \mathcal{C}_Y^\infty)$, the map on stalks $f^\sharp : \mathcal{C}_{Y,f(x)}^\infty \to \mathcal{C}_{X,x}^\infty$ maps the maximal ideal into the maximal ideal.

One can use the established notions to construct spaces by gluing together local patches. Here we only apply this general machinery to make the following definition [1]:

A smooth manifold of dimension n is a locally ringed space $(X, \mathcal{O}_X)$ which admits a covering $X = \bigcup_i U_i$ by open subsets such that each $(U_i, \mathcal{O}_{X|_{U_i}})$ is isomorphic as a locally ringed space to $\{(Y, \mathcal{C}_Y^\infty) \mid Y \in \mathrm{Ouv}(\mathbb{R}^n)\}$. Usually one also requires X to be Hausdorff and paracompact.

1.2.2 Tangent bundle and G-structures on smooth manifolds

Locally ringed spaces give us naturally a notion of a cotangent space at a point by picking out the linear functionals of the stalk at this point. More precisely: Let $(X, \mathcal{O}_X)$ be a locally ringed space, let $x \in X$, let $\mathcal{O}_{X,x}$ be the stalk at x and let $\mathfrak{m}_x$ be its maximal ideal. The tangent space $T_x(X)$ of X at x is the dual of the $\mathcal{O}_{X,x}/\mathfrak{m}_x$-module $\mathfrak{m}_x/\mathfrak{m}_x^2$.

A principal G-bundle over a manifold B with structure group G is a smooth manifold P equipped with a projection $\pi : P \to B$ and a smooth action $G \times P \to P : (g, p) \mapsto pg$ by a Lie group G such that $\pi(pg) = \pi(p)$ for all $p \in P$ and all $g \in G$ and such that G acts freely and transitively on each fiber $P_b = \pi^{-1}(b)$ for every $b \in B$.

The tangent bundle of a manifold M is the vector bundle $T(M) = \{(x, v) | x \in M, v \in T_x(M)\}$. With the tangent bundle $T(M)$ of a manifold M of dimension n there is associated a principal bundle $R(M)$ ("frame bundle"), whose fiber at each $x \in M$ is the set of bases of the tangent space $T_x(M)$, and whose structure group is $\mathrm{GL}(n, \mathbb{R})$. If $G \subset \mathrm{GL}(n, \mathbb{R})$ is a Lie group, a G-structure on M is a subspace $S(M)$ of $R(M)$ that is a principal G-bundle over M.

---

[1]The analogue of a manifold in algebraic geometry is obtained by gluing together affine schemes. An affine scheme consists of the set of prime ideals of a ring (on which a topology can be defined) together with a sheaf of rings on this set.

1.3 Physical introduction

Spacetime in general relativity is a smooth manifold endowed with a G-structure, where G is the Lorentz group [2]. Einstein's equations provide a linkage between some "matter content" and a G-structure. Different "matter contents" give rise in general to different G-structures.

The very rough idea behind gravitational waves is: When "matter content" is changing in time, the corresponding G-structures will also vary in time.

1.4 Keplerian orbit parameters

Unless otherwise stated, we use throughout the text the geometrized unit system, *i.e.* we set $c = G = 1$.

Throughout the text, we often consider masses orbiting in a Keplerian orbit. We denote by $m_1 \geq m_2$ the masses of the two bodies, by $M = m_1 + m_2$ their total mass, by $q = \frac{m_2}{m_1}$ the secondary-to-primary mass ratio and by $\eta = \frac{m_1 m_2}{M^2}$ the symmetric mass ratio. We will throughout the text treat binary problems in the center-of-mass frame. In the center-of-mass-frame the two-body problem reduces to a one-body problem for a particle of reduced mass $\mu = M\eta = M\frac{q}{(1+q)^2}$ orbiting around the total mass M. The mean angular frequency (radians per unit time) is from Kepler's third law

$$\Omega = \sqrt{\frac{M}{a^3}} = \left(\frac{M(1-e)^3}{r_p^3} \right)^{1/2}, \tag{1}$$

where $r_p = a(1-e)$ is the orbit's pericenter distance, a the orbit's semi-major axis and e the orbit's eccentricity. The orbital period is accordingly $T = \frac{2\pi}{\Omega}$. If we set up polar coordinates (r, ϕ) in the plane of the orbit, the orbit equation for any Keplerian orbit reads

$$r = \frac{a(1-e^2)}{1 + e\cos\phi}. \tag{2}$$

1.4.1 Hyperbolic Keplerian orbits

We use the convention that for an hyperbolic orbit the semi-major axis a is negative. The semi-minor axis b of an hyperbola is also the distance from one of the foci of the hyperbola to an asymptote, therefore the semi-minor axis is also called the impact parameter. The following relations characterize an hyperbolic trajectory

$$b = -a(e^2 - 1)^{1/2} \tag{3}$$

$$= \frac{\mu M}{2E}(e^2 - 1)^{1/2} \tag{4}$$

$$= \frac{M}{v^2}(e^2 - 1)^{1/2} \tag{5}$$

$$= \frac{L}{(2E\mu)^{1/2}}. \tag{6}$$

---

[2]In the literature, this viewpoint is in essence known as the tetrad formalism.

Here v is the relative velocity of the two bodies at infinity and $L = b\mu v$ is the angular momentum.

1.4.2 Elliptic Keplerian orbit

The eccentricity of an ellipse is defined through the semiaxes as

$$e^2 = 1 - \frac{b^2}{a^2}. \tag{7}$$

The orbital energy of two bodies on an elliptic Keplerian orbit is inversely proportional to the semi-major axis

$$E = -\frac{\eta M^2}{2a}. \tag{8}$$

The absolute value of the orbital angular momentum is

$$L = \mu\sqrt{Ma(1-e^2)} = \mu\Omega a^2\sqrt{1-e^2}. \tag{9}$$

We can then write for the eccentricity

$$e^2 = 1 + \frac{2EL^2}{M^2\,\mu^3}. \tag{10}$$

1.4.3 Evolution equations of e and a

The evolution equations of the eccentricity and semi-major axis of a bound binary system are obtained by differentiating equations (8) and (10). We obtain

$$\frac{d\log a}{dt} = \frac{1}{a}\frac{da}{dt} = -\frac{\dot{E}}{E} + \frac{2\dot{M}}{M} + \frac{\dot{\eta}}{\eta}, \tag{11}$$

and

$$\frac{de}{dt} = \frac{1-e^2}{2e}\left[-\frac{2\dot{L}}{L} - \frac{\dot{E}}{E} + \frac{2\dot{M}}{M} - \frac{3\dot{\mu}}{\mu}\right]. \tag{12}$$

Under the assumption that $\dot{M} = \dot{\mu} = 0$, the last equation can be rewritten as

$$\frac{de}{dt} = \frac{a(1-e^2)}{e\mu M}\left[\dot{E} - \frac{M^{1/2}}{a^{3/2}(1-e^2)^{1/2}}\dot{L}\right]. \tag{13}$$

2 Aspects of gravitational wave emission

In this section we briefly describe the multipole decomposition formalism in linearised general relativity as given by Thorne [2]. Then this formalism is applied to determine in the mass quadrupole approximation the energy loss, angular momentum loss and energy spectrum for binary systems on elliptic and hyperbolic Keplerian orbits.

2.1 Multipole expansion formalism

In the wave zone, gravitational waves can be treated as linearised perturbations propagating on a flat background metric. This background metric can be characterized by a Minkowskiian coordinate system whose origin coincides with the source. In this coordinate frame the transverse and traceless part of the metric perturbation has the form

$$h_{ij}^{TT} = \frac{1}{r} A_{ij}(t - r, \theta, \phi), \tag{14}$$

where A_{ij} is a traceless and transverse tensor varying in the wave zone rapidly in the radial direction but slowly in the transverse direction. The angular dependence of the radiation field A_{ij} can be decomposed into spherical harmonics. The most suitable set of harmonics are the pure-spin harmonics with well-defined transversality and helicity properties. Because A_{ij} is traceless and transverse, it contains only the transverse and traceless harmonics $\mathbf{T}^{E2,lm}$ and $\mathbf{T}^{B2,lm}$. The purely longitudinal, purely transversal or mixed longitudinal and transversal components are not encountered in standard general relativity, but need to be included in other metric theories of gravity. For $l = 0$ and $l = 1$ there are no transverse traceless harmonics. Therefore the general form of radiation field has the form

$$h_{ij}^{TT} = \frac{1}{r} \sum_{l=2}^{\infty} \sum_{m=-l}^{l} \left[{}^{(l)}I^{lm}(t - r) \, T_{ij}^{E2,lm} + {}^{(l)}S^{lm}(t - r) \, T_{ij}^{B2,lm} \right]. \tag{15}$$

The expansion coefficients ${}^{(l)}I^{lm}$ and ${}^{(l)}S^{lm}$ are the l-th time derivative of I^{lm} and S^{lm}. The components I^{lm} and S^{lm} are said to be responsible for mass multipole radiation and current multipole radiation respectively. For that reason, the leading order terms I^{2m} are responsible for the mass quadrupole radiation, terms associated with S^{2m} are called current quadrupole contributions, terms arising from I^{3m} are called mass octupole contributions, etc. The explicit expression of I^{lm} is given by

$$I^{lm} = \frac{16\pi}{(2l + 1)!!} \left(\frac{(l + 1)(l + 2)}{2l(l - 1)} \right)^{1/2} \mathcal{G}_{A_l} \mathcal{Y}_{A_l}^{lm*}, \tag{16}$$

where $\mathcal{Y}^{lm}$ are symmetric trace free tensors and where $\mathcal{G}_{A_l}$ stands for the mass multipole moments. The general form of the mass multipole moments $\mathcal{G}_{A_l}$ is given by a sum of several integrals involving the energy-stress tensor and spherical Bessel functions, see equation (5.9a) in [2]. Our calculations will only involve the second mass moments, for which $\mathcal{G}_{A_2}$ in the Newtonian limit becomes equation (21). We also don't need expressions for the current multipole contributions S^{lm} in this work.

8

In the next sections we will frequently make use of the following STF tensors

$$
\mathcal{Y}^{22} = \left(\frac{15}{32\pi}\right)^{1/2}
\begin{pmatrix}
1 & i & 0 \\
i & -1 & 0 \\
0 & 0 & 0
\end{pmatrix},
\tag{17}
$$

$$
\mathcal{Y}^{21} = -\left(\frac{15}{32\pi}\right)^{1/2}
\begin{pmatrix}
0 & 0 & 1 \\
0 & 0 & i \\
1 & i & 0
\end{pmatrix},
\tag{18}
$$

$$
\mathcal{Y}^{20} = \left(\frac{5}{16\pi}\right)^{1/2}
\begin{pmatrix}
-1 & 0 & 0 \\
0 & -1 & 0 \\
0 & 0 & 2
\end{pmatrix},
\tag{19}
$$

together with $\mathcal{Y}^{2-m} = (-1)^m \left(\mathcal{Y}^{2m}\right)^*$.

2.1.1 Energy loss

In the multipole formalism the total radiated power is given by

$$
P = \frac{dE}{dt} = \frac{1}{32\pi} \sum_{l=2}^{\infty} \sum_{m=-l}^{l} \left\langle |^{(l+1)}I^{lm}|^2 + |^{(l+1)}S^{lm}|^2 \right\rangle.
\tag{20}
$$

In case of a periodic motion, the brackets denote orbital averaging of the expression. In case of unbound motion, the brackets are to be understood as the integral of the expression over the entire orbit. In what follows, we only consider mass quadrupole radiation, that is, we consider only contributions arising from I^{2m}. If the source is non-relativistic and has a negligible self-gravity, it is possible to express the second mass moment $\mathcal{G}_{a_1 a_2}$ in terms of the Newtonian mass density ρ

$$
\mathcal{G}_{a_1 a_2} = \int d^3 x \, \rho \, x_{a_1} x_{a_2}.
\tag{21}
$$

Then

$$
I^{2m} = \frac{16\pi}{5\sqrt{3}} \int d^3 x \, \rho \, \mathcal{Y}^{2m*}_{a_1 a_2} \, x_{a_1} x_{a_2}
\tag{22}
$$

$$
\equiv \frac{16\pi}{5\sqrt{3}} \int d^3 x \, \rho \, r^2 Y^{2m*}.
\tag{23}
$$

2.1.2 Angular momentum loss

In the multipole expansion formalism, the change in angular momentum of a system due to gravitational wave emission is given by

$$
\frac{dL_j}{dt} = \sum_{l=2}^{\infty} \frac{(l+1)(l+2)}{(l-1)l!(2l+1)!!} \left\langle \epsilon_{jpq} {}^{(l)}\mathcal{G}_{pA_{l-1}} {}^{(l+1)}\mathcal{G}_{qA_{l-1}} \right\rangle
\tag{24}
$$

$$
+ \sum_{l=2}^{\infty} \frac{4l^2(l+2)}{(l-1)(l+1)!(2l+1)!!} \left\langle \epsilon_{jpq} {}^{(l)}\mathcal{S}_{pA_{l-1}} {}^{(l+1)}\mathcal{S}_{qA_{l-1}} \right\rangle.
\tag{25}
$$

In the mass quadrupole approximation this reduces to

$$
\frac{dL_j}{dt} = \frac{2}{5} \left\langle \epsilon_{jpq} {}^{(2)}\mathcal{G}_{pa} {}^{(3)}\mathcal{G}_{qa} \right\rangle.
\tag{26}
$$

2.2 Application to binaries on Keplerian orbits

In this section we calculate, for binaries on a Keplerian orbit and for all $e \geqslant 0$, the energy flux, angular momentum flux and energy spectrum resulting from gravitational wave emission in the mass quadrupole approximation.

The energy emitted by gravitational waves from an elliptic Keplerian binary system was first calculated by Peters & Mathews [3]. The first calculation of the angular momentum loss for elliptic orbits is due to Peters [4]. The analogous expressions for binary systems on hyperbolic orbits were first derived by Hansen [5], both contain minor numerical mistakes. The error in Hansen's expression for the energy flux was rectified by Turner [6] and the first correct expression for the angular momentum flux is found in Junker & Schäfer [7]. The first determination of the elliptic frequency spectrum is given in Peters and Mathews's paper. A first complete calculation of the hyperbolic frequency spectrum is found in DeVittori *et al.* [8], their computation was subsequently corrected by García-Bellido & Nesseris [9]. In subsection (2.2.3) we will settle a minor imprecision that is present throughout [8] and [9].

2.2.1 Energy loss

We choose a coordinate system whose origin coincides with the center of mass of the system and we let the binary lie in the $\theta = \pi/2$-plane. The two masses can then be specified by $(r_1 \cos \phi, r_1 \sin \phi)$ and $(-r_2 \cos \phi, -r_2 \sin \phi)$ with $r_i = \frac{\mu r}{m_i}$. We obtain using equation (23)

$$I^{2m} = \frac{16\pi}{5\sqrt{3}} \left[m_1 \frac{\mu^2 r^2}{m_1^2} Y^{2m*} \left(\frac{\pi}{2}, \phi \right) + m_2 \frac{\mu^2 r^2}{m_2^2} Y^{2m*} \left(\frac{\pi}{2}, \phi + \pi \right) \right]. \qquad (27)$$

Because the $Y^{2\pm1*} \left(\frac{\pi}{2}, \phi \right)$ terms vanish, it is possible to set in the above expression $Y^{2m*} \left(\frac{\pi}{2}, \phi \right)$ equal to $Y^{2m*} \left(\frac{\pi}{2}, \phi + \pi \right)$. Hence we can write

$$I^{2m} = \frac{16\pi}{5\sqrt{3}} \mu r^2 Y^{2m*} \left(\frac{\pi}{2}, \phi \right). \qquad (28)$$

In the quadrupole approximation the power radiated by the system reduces from expression (20) to

$$P = \frac{1}{32\pi} \sum_{m=-2}^{2} |^{(3)}I^{2m}|^2. \qquad (29)$$

The orbit equations

$$r = \frac{r_p(1+e)}{1 + e \cos \phi},$$
$$r^2 \frac{d\phi}{dt} = [Mr_p(1+e)]^{1/2}. \qquad (30)$$

allow the calculation of the time derivatives of I^{2m}. Employing these identities and using the explicit expression of the spherical harmonics Y^{2m*}, the third

time derivatives of I^{2m} read

$$^{(3)}I^{20} = \left(\frac{64\pi}{15}\right)^{1/2} \frac{\mu M^{3/2}}{[r_p(1+e)]^{5/2}} \left(1 + e\cos\phi\right)^2 e\sin\phi,$$

$$^{(3)}I^{2-2} = \left(\frac{32\pi}{5}\right)^{1/2} \frac{\mu M^{3/2}}{[r_p(1+e)]^{5/2}} \left(1 + e\cos\phi\right)^2 \left[-e\sin\phi - 4i(1 + e\cos\phi)\right] e^{2i\phi},$$

$$^{(3)}I^{22} = \left(^{(3)}I^{2-2}\right)^*.$$

The radiated power as a function of ϕ along the orbit is then

$$P(\phi) = \frac{8}{15} \frac{\mu^2 M^3}{[r_p(1+e)]^5} \left(1 + e\cos\phi\right)^4 \left[e^2\sin^2\phi + 12(1 + e\cos\phi)^2\right]. \qquad (31)$$

Note that this expression is valid for all values of $e \geq 0$.

Hyperbolic orbit $e \geq 1$: The asymptotes of an hyperbolic orbit are given by $\cos\psi = -1/e$. Thus the total energy released by a binary on an hyperbolic orbit is

$$E = \int_{-\psi}^{\psi} P(\phi)\frac{dt}{d\phi}\,d\phi \qquad (32)$$

$$= \frac{8}{15}\frac{\eta^2 M^{9/2}}{(r(1+e))^{7/2}} \int_{-\psi}^{\psi} d\phi\,(1 + e\cos\phi)^2 \left[e^2\sin^2\phi + 12(1 + e\cos\phi)^2\right] \qquad (33)$$

$$= \frac{\eta^2 M^{9/2}}{r_p^{7/2}(1+e)^{7/2}} \varrho(e), \qquad (34)$$

where

$$\varrho(e) = \frac{1}{180} \left[(12(96 + 292e^2 + 37e^4)\phi + 48e(96 + 73e^2)\sin\phi \right.$$
$$\left. + 24e^2(71 + 12e^2)\sin 2\phi + 368e^3\sin 3\phi + 33e^4\sin 4\phi\right]_{-\psi}^{\psi}$$
$$= \frac{64}{5} \left[\left(1 + \frac{73}{24}e^2 + \frac{37}{96}e^4\right)\cos^{-1}\left(-\frac{1}{e}\right) + \frac{301}{144}(e^2 - 1)^{1/2}\left(1 + \frac{673}{602}e^2\right)\right].$$

For a parabolic orbit, $e = 1$, the radiated energy becomes

$$E = \frac{85\pi}{12\sqrt{2}}\frac{\eta^2 M^{9/2}}{r_p^{7/2}}. \qquad (35)$$

Elliptic orbit $e < 1$: In case of elliptic orbits, the average of $P(\phi)$ over one orbital period gives

$$\frac{dE}{dt} = P = \frac{\Omega}{2\pi} \int_0^{2\pi} P(\phi)\frac{dt}{d\phi}\,d\phi$$

$$= \frac{8}{15}\frac{1}{(1-e^2)^{7/2}}\frac{\mu^2 M^3}{a^5} \int_0^{2\pi} \frac{d\phi}{2\pi}(1 + e\cos\phi)^2 \left[e^2\sin^2\phi + 12(1 + e\cos\phi)^2\right].$$

After performing the integral we arrive at

$$\frac{dE}{dt} = \frac{32}{5}\frac{\mu^2 M^3}{a^5}\frac{1}{(1-e^2)^{7/2}}\left(1 + \frac{73}{24}e^2 + \frac{37}{96}e^4\right). \qquad (36)$$

11

There is a simple way to deduce the energy loss of a parabolic orbit from the energy loss of an elliptic orbit. The energy radiated per orbit is $E = \frac{2\pi}{\Omega} P$. For a parabolic orbit, the energy radiated per orbit is the total energy radiated. By analytically continuing the orbital parameters to $e = 1$, we then obtain indeed equation (35). An extension of the results from $e < 1$ beyond $e = 1$ is, when resorting to the parametrization used here, not possible.

2.2.2 Angular momentum loss

We now proceed to determine the GW-induced angular momentum loss of a binary on a Keplerian orbit. To this end we choose a coordinate system such that the orbits lies in the $(x, y)-$plane; then we can set $L = L_z$. Therefore we have

$$\frac{dL}{dt} = \frac{2}{5}\left({}^{(2)}\mathcal{G}_{1a}{}^{(3)}\mathcal{G}_{2a} - {}^{(2)}\mathcal{G}_{2a}{}^{(3)}\mathcal{G}_{1a} \right). \tag{37}$$

The second mass moments in our chosen coordinate frame are given by

$$\mathcal{G} = \mu r^2 \begin{bmatrix} \cos^2\phi & \cos\phi\sin\phi & 0 \\ \cos\phi\sin\phi & \sin^2\phi & 0 \\ 0 & 0 & 0 \end{bmatrix}. \tag{38}$$

By making use of the orbit equations (30), we can calculate the required derivatives and obtain

$${}^{(2)}\mathcal{G}_{12} = -\frac{\mu M}{r_p(1+e)}\sin\phi\left[4\cos\phi + e(3 + \cos(2\phi))\right],$$

$${}^{(3)}\mathcal{G}_{12} = -\left(\frac{\mu^2 M^3}{4[r_p(1+e)]^5}\right)^{1/2}(1 + e\cos\phi)^2(5e\cos\phi + 8\cos(2\phi) + 3e\cos(3\phi)),$$

$${}^{(2)}\mathcal{G}_{11} = -\frac{\mu M}{2r_p(1+e)}(3e\cos\phi + 4\cos(2\phi) + e\cos(3\phi)),$$

$${}^{(3)}\mathcal{G}_{11} = \left(\frac{\mu^2 M^3}{[r_p(1+e)]^5}\right)^{1/2}(1 + e\cos\phi)^2(4 + 3e\cos\phi)\sin(2\phi),$$

$${}^{(2)}\mathcal{G}_{22} = \frac{\mu M}{2r_p(1+e)}[7e\cos\phi + 4\cos(2\phi) + e(4e + \cos(3\phi))],$$

$${}^{(3)}\mathcal{G}_{22} = -\left(\frac{\mu^2 M^3}{[r_p(1+e)]^5}\right)^{1/2}(1 + e\cos\phi)^2[8\cos\phi + e(5 + 3\cos(2\phi))]\sin\phi.$$

The angular momentum emitted as a function of ϕ along the orbit is then

$$\frac{dL}{dt} = \frac{4}{5}\frac{\mu^2 M^{5/2}}{[r_p(1+e)]^{7/2}}(1 + e\cos\phi)^3(8 + e^2 + 12e\cos\phi + 3e^2\cos(2\phi)). \tag{39}$$

Hyperbolic orbit $e \geq 1$: The angular momentum loss integrated over the entire hyperbolic orbit is

$$L = \int_{-\psi}^{\psi} \frac{dL}{dt} \frac{dt}{d\phi} \, d\phi \tag{40}$$

$$= \frac{4}{5} \frac{\mu^2 M^2}{[r_p(1+e)]^2} \int_{-\psi}^{\psi} d\phi \, (1 + e\cos\phi)(8 + e^2 + 12e\cos\phi + 3e^2\cos(2\phi)) \tag{41}$$

$$= \frac{4}{5} \frac{\mu^2 M^2}{[r_p(1+e)]^2} \varpi|_{-\psi}^{\psi}, \tag{42}$$

where

$$\varpi = 8\phi + 7e^2\phi + 20e\sin\phi + \frac{5}{2}e^3\sin\phi + \frac{9}{2}e^2\sin(2\phi) + \frac{1}{2}e^3\sin(3\phi).$$

The evaluation of ϖ between $-\psi = -\cos^{-1}(-1/e)$ and $\psi = \cos^{-1}(-1/e)$ gives

$$\varpi|_{-\psi}^{\psi} = 2\left(8 + 7e^2\right)\cos^{-1}\left(-\frac{1}{e}\right) + 2(e^2 - 1)^{1/2}\left(13 + 2e^2\right). \tag{43}$$

For a parabolic orbit, $e = 1$, the emitted angular momentum becomes

$$L = 6\pi \frac{\mu^2 M^2}{r_p^2}. \tag{44}$$

Elliptic orbit $e < 1$: In case of elliptic orbits, the angular momentum change averaged over one orbital period is

$$\frac{dL}{dt} = \frac{\Omega}{2\pi} \int_0^{2\pi} \frac{dL}{dt} \frac{dt}{d\phi} \, d\phi$$

$$= \frac{4}{10\pi} \frac{\mu^2 M^{5/2}}{r_p^{7/2}} \frac{(1-e)^{3/2}}{(1+e)^2} \varpi|_0^{2\pi}.$$

The expression $\varpi|_0^{2\pi}$ evaluates to $2\pi(8 + 7e^2)$ and we have

$$\frac{dL}{dt} = \frac{32}{5} \frac{\mu^2 M^{5/2}}{a^{7/2}} \frac{1}{(1-e^2)^2}\left(1 + \frac{7}{8}e^2\right). \tag{45}$$

Analogous to previous subsection, we can perform an analytical continuation of the above result to $e = 1$, thereby again obtaining the parabolic limit (44) of the hyperbolic case.

2.2.3 Frequency spectrum

In this section we compute for all $e \geq 0$ the frequency spectrum of the radiated power in the mass quadrupole approximation. The key ingredient for this is to perform a Fourier decomposition of the binary's second mass moment.

Elliptic orbit $e < 1$: We parametrize an elliptic Keplerian orbit in the following form

$$x(\beta) = a(\cos u - e), \tag{46}$$
$$y(\beta) = b \sin u. \tag{47}$$

Here a is the semi-major axis and b is the semi-minor axis of the orbit. The eccentric anomaly u is defined by the Kepler equation

$$u - e \sin u = \Omega t \equiv \beta. \tag{48}$$

The second mass moment has then the form

$$\mathcal{G} = \mu \begin{bmatrix} a^2(\cos u - e)^2 & ab(\cos u - e)\sin u & 0 \\ ab(\cos u - e)\sin u & b^2 \sin^2 u & 0 \\ 0 & 0 & 0 \end{bmatrix} \tag{49}$$

$$= \mu \begin{bmatrix} a^2(-2e\cos u + \frac{1}{2}\cos(2u) + e^2 + \frac{1}{2}) & ab(-e\sin u + \frac{1}{2}\sin(2u)) & 0 \\ ab(-e\sin u + \frac{1}{2}\sin(2u)) & \frac{b^2}{2}(1 - \cos(2u)) & 0 \\ 0 & 0 & 0 \end{bmatrix}. \tag{50}$$

The emitted power in the mass quadrupole approximation is obtained from the formulae (16) and (29)

$$P = \frac{8\pi}{75} \sum_{m=-2}^{2} \left\langle \left| {}^{(3)}\mathcal{G}_{a_1 a_2} \left(\mathcal{Y}_{a_1 a_2}^{2m} \right)^* \right|^2 \right\rangle \tag{51}$$

$$= \frac{8\pi}{75} \sum_{m=-2}^{2} \frac{1}{2T} \int_{-T}^{T} dt \left| {}^{(3)}\mathcal{G}_{a_1 a_2} \left(\mathcal{Y}_{a_1 a_2}^{2m} \right)^* \right|^2, \tag{52}$$

with the orbital period T. To find the frequency decomposition of the emitted power we can make use of Parseval's identity. This identity asserts equality between the integral of the norm of a periodic function f and the sum of the norm of the function's Fourier coefficients $\mathcal{F}(f)$

$$\frac{1}{2T} \int_{-T}^{T} dt \, |f(t)|^2 = \sum_{n=-\infty}^{\infty} |\mathcal{F}(f)|^2. \tag{53}$$

The effect of the third derivative is to multiply the power spectrum by $(n\Omega)^6$ while at the same time replacing ${}^{(3)}\mathcal{G}_{a_1 a_2}$ by $\mathcal{G}_{a_1 a_2}$. Hence we can write for the radiated power in the n-th harmonic of the orbital angular frequency

$$P_n = 2 \times \frac{8\pi}{75} (n\Omega)^6 \sum_{m=-2}^{2} \left| \mathcal{F} \left(\mathcal{G}_{a_1 a_2} \left(\mathcal{Y}_{a_1 a_2}^{2m} \right)^* \right) \right|^2 \tag{54}$$

$$= \frac{1}{15} (n\Omega)^6 \, \mu^2 \, \Psi, \tag{55}$$

14

where

$$\Psi = \left| 2a^2 e\, \mathcal{F}(\cos(u)) - \frac{1}{2}\mathcal{F}(\cos(2u))\left(a^2 - b^2\right) \right|^2$$

$$+ 3\left| -2a^2 e\, \mathcal{F}(\cos(u)) + \frac{1}{2}\mathcal{F}(\cos(2u))\left(a^2 + b^2\right) \right|^2 \tag{56}$$

$$+ 12\left| -abe\, \mathcal{F}(\sin(u)) + \frac{ab}{2}\mathcal{F}(\sin(2u)) \right|^2 .$$

The factor 2 appearing in equation (54) accounts for the counting of the negative terms in the sum (53). We now proceed with the calculation of the Fourier coefficients of $\sin(mu)$

$$\mathcal{F}(\sin(mu)) = \frac{1}{2\pi}\int_{-\pi}^{\pi} d\beta\, \sin(mu)\, e^{-in\beta}$$

$$= -\frac{1}{2in\pi}\int_{-\pi}^{\pi} du\, \frac{d}{du}\left(e^{-in\beta}\right)\sin(mu)$$

$$= \frac{m}{2in\pi}\int_{-\pi}^{\pi} du\, e^{-in\beta}\cos(mu)$$

$$= \frac{m}{2in\pi}\int_{-\pi}^{\pi} du\, \cos(n\beta)\cos(mu)$$

$$= \frac{m}{in\pi}\int_{0}^{\pi} du\, \cos(mu)\cos(nu - ne\sin u)$$

$$= \frac{m}{2in}\int_{0}^{\pi}\frac{du}{\pi}\left[\cos(u(n+m) - ne\sin u) + \cos(u(n-m) - ne\sin u)\right].$$

By using the following integral representation of the Bessel functions of the first kind

$$J_n(z) = \int_{0}^{\pi}\frac{du}{\pi}\cos(nu - z\sin u), \tag{57}$$

we arrive at

$$\mathcal{F}(\sin(mu)) = \frac{m}{2in}\left[J_{n+m}(ne) + J_{n-m}(ne)\right]. \tag{58}$$

A similar calculation gives

$$\mathcal{F}(\cos(mu)) = \frac{m}{2n}\left[-J_{n+m}(ne) + J_{n-m}(ne)\right]. \tag{59}$$

By the use of the recurrence relations

$$J_{n-1}(z) + J_{n+1}(z) = \frac{2n}{z}J_n(z), \tag{60}$$

$$J_{n-1}(z) - J_{n+1}(z) = 2J_n'(z), \tag{61}$$

we can express the Fourier coefficients entirely in terms of J_n and its derivative.

We obtain

$$
\begin{aligned}
\mathcal{F}(\sin(u)) &= \frac{1}{ine} J_n(ne), \\
\mathcal{F}(\cos(u)) &= \frac{1}{n} J_n'(ne), \\
\mathcal{F}(\sin(2u)) &= \frac{1}{in} \left[\left(\frac{4}{e^2} - 2 \right) J_n(ne) - \frac{4}{ne} J_n'(ne) \right], \\
\mathcal{F}(\cos(2u)) &= \frac{1}{n} \left[\frac{4}{e} J_n'(ne) - \frac{4}{ne^2} J_n(ne) \right].
\end{aligned}
\tag{62}
$$

We can insert the above Fourier coefficients into expression (56) and we obtain after rearranging

$$
\begin{aligned}
P_n = \ &\frac{16}{15} \frac{n^2 \Omega^6}{e^4} \mu^2 \\
&\times \Big\{ J_n^2(ne) \left[a^4 + b^4 + a^2 b^2 \left(1 + 3n^2 - 6n^2 e^2 + 3n^2 e^4 \right) \right] + \\
&\quad J_n'^2(ne) \left[a^4 \left(e^6 n^2 + n^2 e^2 - 2e^4 n^2 \right) + b^4 n^2 e^2 + a^2 b^2 \left(n^2 e^2 + 3e^2 - e^4 n^2 \right) \right] + \\
&\quad J_n(ne) J_n'(ne) \left[2a^4 \left(ne^3 - ne \right) - 2b^4 ne + a^2 b^2 \left(7ne^3 - 8ne \right) \right] \Big\}.
\end{aligned}
\tag{63}
$$

Parseval's identity allowed us at one stroke to implement the orbital averaging and to decompose the emitted radiation into its harmonics. In appendix (7.1) there is a slightly less straightforward derivation of the frequency spectrum P_n that goes around Parseval's identity.

Hyperbolic orbit $e > 1$: The calculation of the frequency spectrum of an hyperbolic orbits follows the same lines as the calculation of the elliptic one. In fact, by an analytic continuation argument the structure of the hyperbolic frequency spectrum is the same as the elliptic one. However, we will first close our eyes to this fact and present a detailed outline of the calculation. In the end we argue how the result is inferred from the elliptic case.

We parametrize the coordinates on an hyperbolic orbit as

$$
x = a(\cosh u - e), \tag{64}
$$

$$
y = b \sinh u = -a(e^2 - 1)^{\frac{1}{2}} \sinh u, \tag{65}
$$

where the hyperbolic anomaly u satisfies the hyperbolic Kepler equation

$$
e \sinh(u) - u = \Omega t \equiv \frac{\omega}{\nu} t. \tag{66}
$$

Recall that a is strictly negative and that $\Omega = \sqrt{\frac{M}{-a^3}} = \left(\frac{M(e-1)^3}{r_p^3} \right)^{1/2}$. The second mass moment (21) has accordingly the form

$$
\mathcal{G} = \mu \begin{bmatrix} a^2(e^2 - 2e \cosh u + \frac{1}{2}\cosh(2u) + \frac{1}{2}) & -ab(e \sinh u - \frac{1}{2}\sinh(2u)) & 0 \\ -ab(e \sinh u - \frac{1}{2}\sinh(2u)) & \frac{b^2}{2}\cosh(2u) - \frac{b^2}{2} & 0 \\ 0 & 0 & 0 \end{bmatrix}.
\tag{67}
$$

16

We can decompose the total radiated energy in the frequency domain as follows

$$E = \frac{8\pi}{75} \int_{-\infty}^{\infty} dt \sum_{m=-2}^{2} \left| {}^{(3)}\mathcal{G}_{a_1 a_2} \left(\mathcal{Y}_{a_1 a_2}^{2m} \right)^* \right|^2 \tag{68}$$

$$= \frac{1}{2\pi} \frac{8\pi}{75} \int_{-\infty}^{\infty} d\omega \sum_{m=-2}^{2} \left| \left[\widehat{{}^{(3)}\mathcal{G}_{a_1 a_2} \left(\mathcal{Y}_{a_1 a_2}^{2m} \right)^*} \right] \right|^2 \tag{69}$$

$$\equiv \frac{1}{2\pi} \int_{-\infty}^{\infty} d\omega \, P(\omega) = \frac{1}{\pi} \int_{0}^{\infty} d\omega \, P(\omega), \tag{70}$$

where the second equality follows from Plancherel theorem and the hat represents the Fourier transform. We can take the derivative

$$P(\omega) = \frac{8\pi}{75} \omega^6 \sum_{m=-2}^{2} \left| \left(\mathcal{Y}_{a_1 a_2}^{2m} \right)^* \widehat{\mathcal{G}_{a_1 a_2}} \right|^2, \tag{71}$$

and it remains to calculate the Fourier transform of $\mathcal{G}_{a_1 a_2}$, that is

$$\widehat{\mathcal{G}_{a_1 a_2}} = \int_{-\infty}^{\infty} du \, \frac{dt(u)}{du} \, e^{-i\omega t(u)} \, \mathcal{G}_{a_1 a_2}$$

$$= -\frac{1}{i\omega} \int_{-\infty}^{\infty} du \, \frac{d}{du} \left(e^{-i\omega t(u)} \right) \mathcal{G}_{a_1 a_2}.$$

We will outline the remaining calculation for the $\sinh(nu)$ terms

$$\widehat{\sinh(nu)} = -\frac{1}{i\omega} \int_{-\infty}^{\infty} du \, \frac{d}{du} \left(e^{-i\omega t(u)} \right) \sinh(nu)$$

$$= \frac{n}{i\omega} \int_{-\infty}^{\infty} du \, e^{-i\omega t(u)} \cosh(nu)$$

$$= \frac{n}{2i\omega} \int_{-\infty}^{\infty} du \, e^{-i\nu(e \sinh u - u)} \left(e^{nu} + e^{-nu} \right)$$

$$= \frac{n}{2i\omega} \int_{-\infty}^{\infty} du \left(e^{-i\nu e \sinh u + (i\nu + n)u} + e^{-i\nu e \sinh u + (i\nu - n)u} \right).$$

This result can be expressed in terms of modified Bessel functions of the second kind $K_\alpha(x)$. One possible integral representation of $K_\alpha(x)$ has the form (see e.g. page 182 in the Bessel function treatise [10]) [3]

$$K_\alpha(x) = \frac{1}{2} e^{\frac{1}{2}\alpha\pi i} \int_{-\infty}^{\infty} dt \, e^{-ix \sinh t + \alpha t}. \tag{72}$$

---

[3]In [8] and [9] it is asserted that the Hankel functions of the first kind $H_\alpha^{(1)}(z)$ have the integral representation

$$H_\alpha^{(1)}(z) = \frac{1}{\pi i} \int_{-\infty}^{\infty} dt \, e^{z \sinh t - \alpha t}.$$

However, the Hankel function of the first kind $H_\alpha^{(1)}(z)$ is actually defined by integrating the above integrand along the contour $[-\infty, 0] \cup [i\pi, i(\pi + \infty)]$, and the resulting integral representation would then only be valid for $|\arg(z)| < \frac{\pi}{2}$ (see e.g. page 178 in [10]).

Using the above integral representation of $K_\alpha(x)$ we can write for the Fourier transforms [4]

$$\widehat{\sinh(nu)} = \frac{n}{i\omega} e^{\frac{1}{2}\nu\pi} e^{-\frac{1}{2}n\pi i} \left[K_{i\nu+n}\left(\nu e\right) + e^{i\pi n} K_{i\nu-n}\left(\nu e\right) \right]. \tag{73}$$

For the relevant terms for $\widehat{\mathcal{G}_{a_1 a_2}}$ we get

$$\begin{aligned}
\widehat{\sinh(u)} &= -\frac{1}{\omega} e^{\frac{1}{2}\nu\pi} \left[K_{i\nu+1}\left(\nu e\right) - K_{i\nu-1}\left(\nu e\right) \right], \\
\widehat{\sinh(2u)} &= -\frac{2}{i\omega} e^{\frac{1}{2}\nu\pi} \left[K_{i\nu+2}\left(\nu e\right) + K_{i\nu-2}\left(\nu e\right) \right].
\end{aligned} \tag{74}$$

The calculation of $\widehat{\cosh(nu)}$ proceeds the same way and one finds

$$\widehat{\cosh(nu)} = \frac{n}{i\omega} e^{\frac{1}{2}\nu\pi} e^{-\frac{1}{2}n\pi i} \left[K_{i\nu+n}\left(\nu e\right) - e^{i\pi n} K_{i\nu-n}\left(\nu e\right) \right], \tag{75}$$

so that we have

$$\begin{aligned}
\widehat{\cosh(u)} &= -\frac{1}{\omega} e^{\frac{1}{2}\nu\pi} \left[K_{i\nu+1}\left(\nu e\right) + K_{i\nu-1}\left(\nu e\right) \right], \\
\widehat{\cosh(2u)} &= -\frac{2}{i\omega} e^{\frac{1}{2}\nu\pi} \left[K_{i\nu+2}\left(\nu e\right) - K_{i\nu-2}\left(\nu e\right) \right].
\end{aligned} \tag{76}$$

We can now use the recurrence relations

$$\begin{aligned}
K_\alpha(x) &= -\frac{x}{2\alpha} [K_{\alpha-1}(x) - K_{\alpha+1}(x)], \\
K'_\alpha(x) &= -\frac{1}{2} [K_{\alpha-1}(x) + K_{\alpha+1}(x)],
\end{aligned} \tag{77}$$

to derive the following identities

$$\begin{aligned}
K_{\alpha+2}(x) + K_{\alpha-2}(x) &= \left(\frac{4\alpha^2}{x^2} + 2 \right) K_\alpha(x) - \frac{4}{x} K'_\alpha(x), \\
K_{\alpha+2}(x) - K_{\alpha-2}(x) &= -\frac{4\alpha}{x} K'_\alpha(x) + \frac{4\alpha}{x^2} K_\alpha(x).
\end{aligned} \tag{78}$$

Combining the above we arrive at

$$\begin{aligned}
\widehat{\sinh(u)} &= -\frac{2i}{\omega e} e^{\frac{1}{2}\nu\pi} K_{i\nu}\left(\nu e\right), \\
\widehat{\sinh(2u)} &= -\frac{2}{i\omega} e^{\frac{1}{2}\nu\pi} \left[\left(\frac{-4}{e^2} + 2 \right) K_{i\nu}\left(\nu e\right) - \frac{4}{\nu e} K'_{i\nu}\left(\nu e\right) \right], \\
\widehat{\cosh(u)} &= \frac{2}{\omega} e^{\frac{1}{2}\nu\pi} K'_{i\nu}\left(\nu e\right), \\
\widehat{\cosh(2u)} &= \frac{8}{e\omega} e^{\frac{1}{2}\nu\pi} \left[K'_{i\nu}\left(\nu e\right) - \frac{1}{\nu e} K_{i\nu}\left(\nu e\right) \right].
\end{aligned} \tag{79}$$

---

[4]Strictly speaking, when $\mathrm{Re}(\alpha) \in \mathbb{Z}$, the function $K_\alpha(x)$ has to be interpreted as the limiting value $\lim_{\beta \to \alpha} K_\beta(x)$ for $\mathrm{Re}(\beta) \in \mathbb{R} \setminus \mathbb{Z}$.

From equation (71) for the radiated power in the frequency domain we find

$$P(\omega) = \frac{1}{30}\,\omega^6\,\mu^2\,\Pi, \tag{80}$$

where

$$
\begin{aligned}
\Pi = {} & \left| 2a^2e\,\widehat{\cosh(u)} - \frac{1}{2}\widehat{\cosh(2u)}\left(a^2+b^2\right)\right|^2 \\
& + 3\left| -2a^2e\,\widehat{\cosh(u)} + \frac{1}{2}\widehat{\cosh(2u)}\left(a^2-b^2\right)\right|^2 \\
& + 12\left| abe\,\widehat{\sinh(u)} - \frac{ab}{2}\,\widehat{\sinh(2u)}\right|^2 .
\end{aligned}
\tag{81}
$$

By plugging in the explicit expressions of the Fourier transforms (79), we can bring $P(\omega)$ into a similar form as (63). We obtain after factoring out terms

$$
\begin{aligned}
P(\omega) = {} & \frac{64}{30}\,\frac{\omega^2}{e^4}\,\mu^2\,\exp(\nu\pi) \\
& \times \Big\{ K_{i\nu}^2\left(\nu e\right)\left[(a^4+b^4)\Omega^2 + a^2b^2\left(3\omega^2 - 6\omega^2e^2 + 3\omega^2e^4 - \Omega^2\right)\right] + \\
& \quad K_{i\nu}'^2\left(\nu e\right)\left[a^4\left(e^2\omega^2 + \omega^2e^6 - 2\omega^2e^4\right) + b^4\omega^2e^2 + a^2b^2\left(-\omega^2e^2 + \omega^2e^4 + 3\Omega^2e^2\right)\right] + \\
& \quad K_{i\nu}\left(\nu e\right) K_{i\nu}'\left(\nu e\right)\left[2a^4\left(e^3-e\right)\omega\Omega - 2b^4\omega\Omega e + a^2b^2\left(-7e^3 + 8e\right)\omega\Omega\right]\Big\}.
\end{aligned}
\tag{82}
$$

The similarity of the calculation and final expressions of the elliptic and hyperbolic case is not a surprise. In fact, for a deduction of the hyperbolic frequency spectrum from the elliptic one, it suffices to modify the calculation of the elliptic case as follows:

1. The hyperbolic Kepler equation (66) is obtained from the elliptic one (equation (48)) by setting $u \mapsto iu$. Hence $\sin(nu) \mapsto i\sinh(nu)$ and $\cos(nu) \mapsto \cosh(nu)$.

2. The Fourier coefficients become Fourier transforms and $n\Omega \mapsto \omega$.

3. The energy radiated per orbit into the n-th harmonic, *i.e.* $E(n) = \frac{2\pi}{\Omega}P(n)$, becomes the total energy radiated into the frequency ν.

The power emitted at zero frequency is non-zero for $e > 1$; this effect is called gravitational wave memory. To see this, we expand $K_0\left(\nu e\right)$ and $K_0'\left(\nu e\right)$ to first order in ν around $\nu = 0$. The result is (see *e.g.* formula (9.6.13) in Abramowitz and Stegun [11])

$$K_0\left(\nu e\right) = -\gamma - \log\left(\frac{e}{2}\right) - \log(\nu) + \mathcal{O}(\nu^2), \tag{83}$$

$$K_0'\left(\nu e\right) = -\frac{1}{e\nu} + \frac{e\nu}{4}\left(1 - 2\gamma - 2\log\left(\frac{e}{2}\right) - 2\log(\nu)\right) + \mathcal{O}(\nu^2), \tag{84}$$

where γ denotes Euler's constant. Inserting the above expressions into the equation (81) and then taking the limit of equation (80) towards $\omega = 0$ gives

$$\lim_{\omega\to 0} P(\omega) = \frac{32}{5}\frac{\mu^2 M^2(e^2-1)}{a^2e^4}. \tag{85}$$

19

The gravitational memory effect that results from hyperbolic encounters has been calculated up to 1.5 post-Newtonian accuracy in De Vittori *et al.* [12]. They find that only the cross polarization state of the radiation field contributes to the memory effect and that in the Newtonian limit this state behaves as $|h_\times|^2 \propto \frac{\mu^2 M^2}{a^2} \frac{e^2-1}{e^4}$, with agrees with expression (85).

In figure (1) we plot the frequency spectrum (82) for eccentricities ranging from $e = 1.5$ to $e = 3$. Both the value of the frequency $\bar{\omega}$, where $P(\bar{\omega})$ is maximal, and the value $P(\bar{\omega})$ decrease with increasing hyperbolicity. As expected, the power emitted at zero frequency is non-zero for $e > 1$.
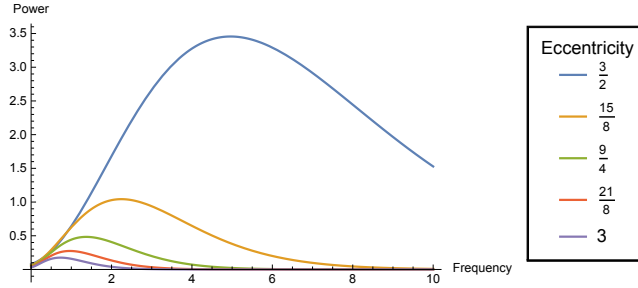

Figure 1: The frequency spectrum of the power emitted by gravitational waves from two masses $(q = 0.5)$ during an hyperbolic encounter with eccentricities ranging from $e = 1.5$ to $e = 3$. In this plot a unit system is used where $G = c = M = |a| = 1$.

Parabolic orbit $e = 1$: In this section we determine the parabolic energy spectrum by taking the appropriate limit of the corresponding elliptic (or hyperbolic) result.

The total energy emitted into the n-harmonic $E(n) = \frac{2\pi}{\Omega} P(n)$ during one elliptic orbit is equivalent the energy spectrum $\frac{dE(\omega)}{d\omega}$ multiplied by Ω,

$$\left. \frac{dE(\omega)}{d\omega} \right|_{\text{elliptic}} = \frac{2\pi}{\Omega^2} P(n), \tag{86}$$

and given that the involved expressions are subject to the substitution

$$n \mapsto \frac{\omega}{\Omega} = \frac{r_p^{3/2}}{M^{1/2}} \frac{\omega}{(1-e)^{3/2}} \equiv \tilde{\nu} \frac{1}{(1-e)^{3/2}}. \tag{87}$$

We recast the elliptic energy spectrum using expressions (55), (56) and (62) to the form

$$\left. \frac{dE(\omega)}{d\omega} \right|_{\text{elliptic}} = \frac{8\pi}{15} \mu^2 \omega^4 \frac{r_p^4}{(1-e)^4} \Psi, \tag{88}$$

where

$$\Psi = \left| \frac{(1-e)^{3/2}}{\tilde{\nu}} J_n(ne) \right|^2$$

$$+ 3 \left| 2 J_n'(ne) \frac{1-e^2}{e} - \frac{(1-e)^{3/2}}{\tilde{\nu}} \frac{2-e^2}{e^2} J_n(ne) \right|^2 \tag{89}$$

$$+ 12 \left| \frac{(1-e^2)^{\frac{3}{2}}}{e^2} J_n(ne) - \frac{(1-e^2)^{\frac{1}{2}}(1-e)^{3/2}}{e\tilde{\nu}} J_n'(ne) \right|^2.$$

In the limit of $e \to 1$, $n \to \infty$. Therefore we need $J_n(nz)$ and $J_n'(nz)$ as $n \to \infty$. We have the following asymptotic expansion for $J_n(nz)$ (this Bessel function expansion and the ones to follow are derived in Olver [13])

$$J_n(nz) \sim \left(\frac{4\zeta}{1-z^2} \right)^{1/4} \left\{ \frac{\mathrm{Ai}(n^{2/3}\zeta)}{n^{1/3}} \sum_{s=0}^{\infty} \frac{A_s(\zeta)}{n^{2s}} + \frac{\mathrm{Ai}'(n^{2/3}\zeta)}{n^{5/3}} \sum_{s=0}^{\infty} \frac{B_s(\zeta)}{n^{2s}} \right\}, \tag{90}$$

as $n \to \infty$ and provided that $|\arg(z)| < \pi$. In the above formula Ai denotes the Airy function of the first kind and ζ is given by

$$\frac{2}{3}(-\zeta)^{3/2} = (z^2-1)^{1/2} - \arccos\left(\frac{1}{z} \right). \tag{91}$$

The coefficients A_s and B_s are given by

$$A_s(\zeta) = \sum_{m=0}^{2s} b_m \zeta^{-\frac{3}{2}m} U_{2s-m}, \quad \zeta^{\frac{1}{2}} B_s(\zeta) = -\sum_{m=0}^{2s+1} a_m \zeta^{-\frac{3}{2}m} U_{2s-m+1}, \tag{92}$$

in which $U_0 = 1$ and with $u = (1-z^2)^{-\frac{1}{2}}$

$$U_{s+1} = \frac{1}{2} u^2 (1-u^2) \frac{dU_s}{du} + \frac{1}{8} \int_0^u du \, U_s (1-5u^2).$$

21

The remaining coefficients are recursively defined by $a_0 = b_0 = 1$ and

$$a_s = \frac{(2s+1)(2s+3)\cdots(6s-1)}{s!\,(144)^s}, \quad b_s = -\frac{6s+1}{6s-1}a_s. \tag{93}$$

The Bessel function derivative $J_n'(ne)$ has the asymptotic expansion

$$J_n'(nz) \sim -\frac{2}{z}\left(\frac{1-z^2}{4\zeta}\right)^{1/4}\left\{\frac{\mathrm{Ai}(n^{2/3}\zeta)}{n^{4/3}}\sum_{s=0}^{\infty}\frac{C_s(\zeta)}{n^{2s}} + \frac{\mathrm{Ai}'(n^{2/3}\zeta)}{n^{2/3}}\sum_{s=0}^{\infty}\frac{D_s(\zeta)}{n^{2s}}\right\}, \tag{94}$$

where

$$C_s(\zeta) = \chi(\zeta)A_s(\zeta) + A_s'(\zeta) + \zeta B_s(\zeta),$$
$$D_s(\zeta) = A_s(\zeta) + \chi(\zeta)B_{s-1}(\zeta) + B_{s-1}'(\zeta),$$

and

$$\chi(\zeta) = \frac{4 - z^2\left(\frac{4\zeta}{1-z^2}\right)^{3/2}}{16\zeta}.$$

Let us also aim to specialize the hyperbolic energy spectrum to the parabolic case. From expressions (70), (79), (80) and (81) we deduce that the hyperbolic energy spectrum has the form

$$\left.\frac{dE(\omega)}{d\omega}\right|_{\text{hyperbolic}} = \frac{8}{15\pi}\omega^4\mu^2\left(\frac{r_p}{1-e}\right)^4 e^{\nu\pi}\,\Pi, \tag{95}$$

where

$$\Pi = \left|\frac{(e-1)^{3/2}}{\tilde{\nu}}K_{i\nu}(\nu e)\right|^2$$
$$+ 3\left|2K_{i\nu}'\frac{1-e^2}{e} - \frac{(e-1)^{3/2}}{\tilde{\nu}}\frac{2-e^2}{e^2}K_{i\nu}(\nu e)\right|^2 \tag{96}$$
$$+ 12\left|\frac{(e^2-1)^{\frac{3}{2}}}{e^2}K_{i\nu}(\nu e) - \frac{(e^2-1)^{\frac{1}{2}}(e-1)^{3/2}}{e\tilde{\nu}}K_{i\nu}'(\nu e)\right|^2.$$

To obtain the parabolic energy spectrum, we need to accommodate to the limit as $\nu = \frac{\tilde{\nu}}{(e-1)^{3/2}} \to \infty$.

The modified Bessel functions of the second kind are related to the purely imaginary Hankel functions

$$K_\alpha(z) = \frac{1}{2}\pi i e^{\frac{\alpha\pi i}{2}}H_\alpha^{(1)}(iz); \tag{97}$$

in our case

$$K_{i\nu}(\nu e) = \frac{1}{2}\pi i e^{-\frac{\nu\pi}{2}}H_{i\nu}^{(1)}(i\nu e). \tag{98}$$

22

The respective asymptotic expansions for the Hankel function of the first kind are

$$H_n^{(1)}(nz) \sim 2e^{-\frac{\pi i}{3}} \left(\frac{4\zeta}{1-z^2}\right)^{1/4} \left\{ \frac{\mathrm{Ai}(e^{\frac{2\pi i}{3}} n^{2/3}\zeta)}{n^{1/3}} \sum_{s=0}^{\infty} \frac{A_s(\zeta)}{n^{2s}} \right.$$

$$\left. + \frac{e^{\frac{2\pi i}{3}} \mathrm{Ai}'(e^{\frac{2\pi i}{3}} n^{2/3}\zeta)}{n^{5/3}} \sum_{s=0}^{\infty} \frac{B_s(\zeta)}{n^{2s}} \right\}, \tag{99}$$

$$H_n^{(1)'}(nz) \sim \frac{4e^{\frac{2\pi i}{3}}}{z} \left(\frac{1-z^2}{4\zeta}\right)^{1/4} \left\{ \frac{\mathrm{Ai}(e^{\frac{2\pi i}{3}} n^{2/3}\zeta)}{n^{4/3}} \sum_{s=0}^{\infty} \frac{C_s(\zeta)}{n^{2s}} \right.$$

$$\left. + \frac{e^{\frac{2\pi i}{3}} \mathrm{Ai}'(e^{\frac{2\pi i}{3}} n^{2/3}\zeta)}{n^{2/3}} \sum_{s=0}^{\infty} \frac{D_s(\zeta)}{n^{2s}} \right\}. \tag{100}$$

The expansions (90), (94), (99) and 100) hold with n replaced by $\xi = ne^{i\theta}$, provided that $\theta < |\frac{\pi}{2}|$ (as we need purely complex orders, we will resort to the limiting value). Therefore we obtain the desired expansions

$$K_{i\nu}(\nu e) \sim \pi e^{-\frac{\nu\pi}{2}} \left(\frac{4\zeta}{1-e^2}\right)^{1/4} \left\{ \frac{\mathrm{Ai}(-\nu^{2/3}\zeta)}{\nu^{1/3}} \sum_{s=0}^{\infty} (-1)^s \frac{A_s(\zeta)}{\nu^{2s}} \right.$$

$$\left. + \frac{\mathrm{Ai}'(-\nu^{2/3}\zeta)}{\nu^{5/3}} \sum_{s=0}^{\infty} (-1)^s \frac{B_s(\zeta)}{\nu^{2s}} \right\} \tag{101}$$

$$K_{i\nu}'(\nu e) \sim -\pi e^{-\frac{\nu\pi}{2}} \frac{2}{e} \left(\frac{1-e^2}{4\zeta}\right)^{1/4} \left\{ \frac{\mathrm{Ai}(-\nu^{2/3}\zeta)}{\nu^{4/3}} \sum_{s=0}^{\infty} (-1)^s \frac{C_s(\zeta)}{\nu^{2s}} \right.$$

$$\left. - \frac{\mathrm{Ai}'(-\nu^{2/3}\zeta)}{\nu^{2/3}} \sum_{s=0}^{\infty} (-1)^s \frac{D_s(\zeta)}{\nu^{2s}} \right\}. \tag{102}$$

We will now specialize the above expressions to the limit of $e \to 1$. A power counting argument shows that, in this limit, only the leading term in each Bessel function expansion evaluates to a non-zero value in the spectra (88) and (95). Expanding equation (91) around $z = 1$ yields the following value for ζ

$$\zeta = 2^{\frac{1}{3}}(1-z). \tag{103}$$

Applying the above limit of ζ and restoring $n = \tilde{\nu} \frac{1}{(1-e)^{3/2}}$ and $\nu = \frac{\tilde{\nu}}{(e-1)^{3/2}}$ in the respective variables we find the following expressions for the leading terms

of the Bessel function expansions (90), (94), (101) and (102)

$$J_n(ne) \sim \left(\frac{2}{\tilde{\nu}}\right)^{1/3} (1-e)^{\frac{1}{2}} \, \text{Ai}(2^{\frac{1}{3}} \tilde{\nu}^{\frac{2}{3}}), \tag{104}$$

$$J_n'(ne) \sim -\left(\frac{2}{\tilde{\nu}}\right)^{2/3} \frac{1-e}{e} \, \text{Ai}'(2^{\frac{1}{3}} \tilde{\nu}^{\frac{2}{3}}), \tag{105}$$

$$K_{i\nu}(\nu e) \sim \pi e^{-\frac{\nu\pi}{2}} \left(\frac{2}{\tilde{\nu}}\right)^{1/3} (e-1)^{\frac{1}{2}} \, \text{Ai}(2^{\frac{1}{3}} \tilde{\nu}^{\frac{2}{3}}), \tag{106}$$

$$K_{i\nu}'(\nu e) \sim \pi e^{-\frac{\nu\pi}{2}} \left(\frac{2}{\tilde{\nu}}\right)^{2/3} \frac{e-1}{e} \, \text{Ai}'(2^{\frac{1}{3}} \tilde{\nu}^{\frac{2}{3}}). \tag{107}$$

By exploiting the above formulae it is now elementary to verify that the parabolic limit of the elliptic energy spectrum and the parabolic limit of the hyperbolic energy spectrum coincide. Both limits give the parabolic energy spectrum as

$$\begin{aligned}
\left.\frac{dE(\omega)}{d\omega}\right|_{\text{parabolic}} = {}& \frac{128\pi}{5} \, \omega^4 \, \mu^2 \, r_p^4 \\
& \times \left\{ \text{Ai}^2(2^{\frac{1}{3}} \tilde{\nu}^{\frac{2}{3}}) \left(\frac{2}{\tilde{\nu}}\right)^{2/3} \left(2 + \frac{1}{12\tilde{\nu}^2}\right) \right. \\
& \left. + \text{Ai}'^2(2^{\frac{1}{3}} \tilde{\nu}^{\frac{2}{3}}) \left(\frac{2}{\tilde{\nu}}\right)^{4/3} \right. \\
& \left. + \text{Ai}(2^{\frac{1}{3}} \tilde{\nu}^{\frac{2}{3}}) \, \text{Ai}'(2^{\frac{1}{3}} \tilde{\nu}^{\frac{2}{3}}) \frac{1}{\tilde{\nu}^2} \right\}.
\end{aligned} \tag{108}$$

$$J_n(nz) \sim \left(\frac{4\zeta}{1-z^2}\right)^{1/4} \frac{\mathrm{Ai}(n^{2/3}\zeta)}{n^{1/3}}. \tag{109}$$

Under the validity of the above approximation we obtain [5]

$$J_n(nz) \sim 2^{\frac{1}{3}} n^{-\frac{1}{3}} \mathrm{Ai}(n^{\frac{2}{3}} 2^{\frac{1}{3}} (1-z)). \tag{112}$$

The substitution $n = \tilde{\nu} \frac{1}{(1-e)^{3/2}}$ in expression (112) yields

$$J_n(ne) \sim \left(\frac{2}{\tilde{\nu}}\right)^{1/3} (1-e)^{\frac{1}{2}} \mathrm{Ai}(\tilde{\nu}^{\frac{2}{3}} 2^{\frac{1}{3}}). \tag{113}$$

---

[5] By employing the principle of stationary phase to the integral representation (57) it is straightforward to derive the following asymptotic expansion of $J_n(nz)$, which is valid for nearly equal nz and n (both being large) and for $nz < n$ (see *e.g.* page 249 in [10])

$$J_n(nz) \sim \frac{1}{\pi} \left(\frac{2(1-z)}{3z}\right)^{\frac{1}{2}} K_{\frac{1}{3}}\left(\frac{2^{\frac{3}{2}}}{3z^{\frac{1}{2}}} n(1-z)^{\frac{3}{2}}\right). \tag{110}$$

One can express the Airy function in (112) in terms of a modified Bessel function, thereby obtaining

$$J_n(nz) \sim \frac{1}{\pi} \frac{2^{\frac{1}{2}}(1-z)^{\frac{1}{2}}}{3^{\frac{1}{2}}} K_{\frac{1}{3}}\left(\frac{2^{\frac{3}{2}}}{3} n(1-z)^{\frac{3}{2}}\right). \tag{111}$$

This expression coincides with the expression (110) when adopting the limiting case $z \to 1$.

2.3 Formation of binaries through gravitational wave capture

When two black holes on an hyperbolic trajectory have a near encounter, they may release sufficiently energy through gravitational waves to form a bound binary system.

In the center of mass system, the initial energy of two non-interacting masses is $E_{\text{ini}} = \frac{\mu v^2}{2} = \frac{\mu M (e^2-1)^{1/2}}{2b}$, while the angular momentum of the system is $\mu v b$. Conservation of energy and angular momentum of the system before and after the transition from an hyperbolic to an elliptic orbit gives the equations

$$E_{\text{fin}} = E_{\text{ini}} - E_{\text{GW}}, \tag{114}$$

$$L_{\text{fin}} = \mu v b - L_{\text{GW}}, \tag{115}$$

where the rightmost terms are the released energy through gravitational waves during an hyperbolic encounter (equation (34)) and the amount of angular momentum lost during an hyperbolic encounter (equation (42)) respectively. For there to form a bound binary system, the energy after the encounter E_{fin} must be negative. By the use of the hyperbolic orbit parameters, we can write E_{GW} in terms of μ, M, e and b. Then we can obtain from the condition $E_{\text{ini}} = E_{\text{GW}}$ the maximal impact parameter for capture b_{max} as a function of μ, M and e. It is

$$b_{\text{max}} = \left(\frac{4\mu^2 \varrho(e)^2}{M} \right)^{1/5} \frac{(e-1)^{1/2}}{(e+1)^{9/10} |1-e|^{7/5}}. \tag{116}$$

In figure (2) we plot the maximal impact parameter for capture as a function of the eccentricity for binary systems with different mass ratios. We see that the disk of capture decreases as the eccentricity increases and increases as the mass ratio increases. When captured, the orbital semi-major axis after the encounter is

$$a_0 = \frac{\mu M}{2|E_{\text{fin}}|}, \tag{117}$$

while the orbital eccentricity after the encounter reads

$$e_0^2 - 1 = \frac{2 E_{\text{fin}} L_{\text{fin}}^2}{M^2 \mu^3}. \tag{118}$$

2.4 Orbital evolution equations for binaries on elliptic orbits

The orbital parameters of a binary system are affected due to the release of gravitational waves. We derive the evolution equations of the semi-major axis and the eccentricity for binaries on an elliptic Keplerian orbit.

Substituting the energy loss equation (36) into the evolution equation (11) one finds the gravitational wave driven evolution of the semi-major axis

$$\frac{da}{dt} = -\frac{64}{5} \frac{\mu M^2}{a^3} \frac{1}{(1-e^2)^{7/2}} \left(1 + \frac{73}{24}e^2 + \frac{37}{96}e^4 \right). \tag{119}$$
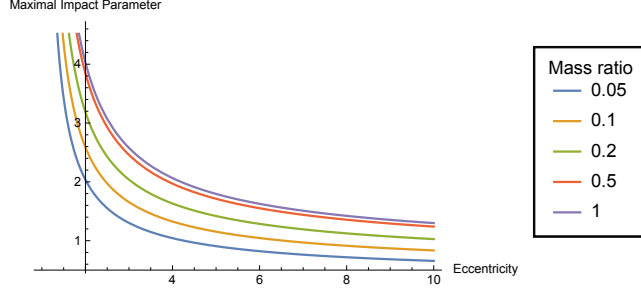
Figure 2: Maximal impact parameter for gravitational wave capture as a function of the eccentricity of the initially hyperbolic orbit. A unit system is used where $G = c = M = 1$.

Substituting both (36) and (45) into the evolution equation (13) one finds the gravitational wave driven evolution of the orbital eccentricity

$$\frac{de}{dt} = -\frac{304}{15} \frac{\mu M^2}{a^4} \frac{e}{(1 - e^2)^{5/2}} \left(1 + \frac{121}{304} e^2\right). \tag{120}$$

Combining equations (119) and (120) gives

$$\frac{da}{de} = \frac{12}{19} \frac{a}{e} \frac{1 + (73/24)e^2 + (37/96)e^4}{(1 - e^2)\left(1 + \frac{121}{304}e^2\right)}. \tag{121}$$

The solution of the differential equation (121) is

$$a(e) = c_0 \frac{e^{12/19}}{1 - e^2} \left(1 + \frac{121}{304} e^2\right)^{870/2299}, \tag{122}$$

where c_0 depends on the initial semi-major axis a_0 and the initial orbital eccentricity e_0. By requiring $a(e_0) = a_0$, we can set

$$c_0 = a_0 \left(1 - e_0^2\right) e_0^{-12/19} \left(1 + \frac{121}{304} e_0^2\right)^{-\frac{870}{2299}}.$$

From the orbit equation (1) we can determine the orbital frequency as a function of the eccentricity

$$\frac{\omega}{\omega_0} = \left[\left(\frac{e}{e_0}\right)^{\frac{12}{19}} \frac{1 - e_0^2}{1 - e^2} \left(\frac{1 + \frac{121}{304}e^2}{1 + \frac{121}{304}e_0^2}\right)^{\frac{870}{2299}}\right]^{-3/2}, \tag{123}$$

with the initial orbital frequency $\omega_0 = \sqrt{\frac{M}{a_0^3}}$.

To find the time to coalescence τ we can integrate the inverse to equation (120) by requiring that $e(\tau) = 0$, for at coalescence the eccentricity goes to zero. The time to merger for a binary system that is only subject to gravitational wave emission is thus given by the integral

$$\tau = \frac{15}{304} \frac{1}{\mu M^2} \int_0^{e_0} de \, a(e)^4 \frac{(1 - e^2)^{5/2}}{e} \left(1 + \frac{121}{304} e^2\right)^{-1} \tag{124}$$

$$= \frac{15}{304} \frac{1}{\mu M^2} c_0^4 \int_0^{e_0} de \, \frac{e^{29/19}}{(1 - e^2)^{3/2}} \left(1 + \frac{121}{304} e^2\right)^{1181/2299}. \tag{125}$$

27

3 Binary Black Holes in gaseous environments

3.1 Active galactic nuclei

3.1.1 Simplified model of AGN

In our setup of a disk we make many simplifying assumptions. We assume that the disk is axial-symmetric, is geometrically thin and that it is not self-gravitating. The last assumptions means that the motion of the gas may be approximated as being Keplerian, that is, the orbital frequency of the gas at the radius r is $\Omega = \left(\frac{M_{\text{SMBH}}}{r^3}\right)^{1/2}$, where M_{SMBH} is the mass of the central object.

The equation for hydrostatic equilibrium in the vertical direction for a geometrically thin disk in a central gravitational potential is

$$\frac{dp}{dz} = -\rho \frac{M_{\text{SMBH}} z}{r^3}, \tag{126}$$

where p and ρ are the pressure and mass density (which are functions of the radius r and height z of the disk). We assume the disk to be isothermal in the vertical direction; this amounts to setting $c_s^2 = \frac{p}{\rho}$, where c_s is the sound speed (dependent on r, but independent of z). Hence we obtain for the mass density

$$\rho = \rho_0 e^{-\frac{z^2}{2h^2}}, \tag{127}$$

with the density at the equatorial plane ρ_0 and with the disk scale height

$$h = \frac{c_s r^{3/2}}{M_{\text{SMBH}}^{1/2}} = \frac{c_s}{\Omega}. \tag{128}$$

Hence we can write for the sound speed

$$c_s = h\Omega = \left(\frac{h}{r}\right)\left(\frac{M_{\text{SMBH}}}{r}\right)^{1/2}; \tag{129}$$

the quantity $\frac{h}{r}$ is called the disk aspect ratio, which for geometrically thin disks is $\ll 1$. In the AGN model outlined in Thompson *et al.* [14], the mass of the gas in the disk M_g is set to $2f_g \sigma^2 r$, where σ stands for the stellar velocity dispersion and where $f_g = \frac{\Sigma_g}{\Sigma}$ is the gas surface density Σ_g divided by the total surface density Σ. The gas surface density Σ_g is then obtained from the relation $\frac{dM_g}{dr} = 2\pi r \Sigma_g$, *i.e.*

$$\Sigma_g = f_g \frac{\sigma^2}{\pi r}. \tag{130}$$

There is empirical evidence for a correlation between the mass M_{SMBH} of the supermassive black hole and the stellar velocity dispersion σ. We adopt the $M_{\text{SMBH}} - \sigma$ relation from Kormendy & Ho [15]

$$M_{\text{SMBH}} = 3.7 \times 10^{15} \times \sigma^{4.38}. \tag{131}$$

For our purposes an AGN disk is fully characterized by its central mass M_{SMBH}, its surface gas ratio f_g, its aspect ratio h/r and its viscosity parameter α (see next paragraph). Whenever in later sections we speak of a disk's sound speed and a disk's surface density at a given radius r, we will resort to expressions (129) and (130) to calculate the corresponding quantities at r.

3.1.2 A little on accretion disks

Viscous Torque in the Disc   Because the angular velocity of the accretion disk varies with radius, a viscous torque is acting on the gas. This torque represents the amount of angular momentum crossing the disk circumference at radius r per unit time due to the action of viscosity. The shear stress is $\tau = \rho \nu r \frac{d\Omega}{dr}$, where ν is the dynamical viscosity and ρ the mass density (depending on r). This leads to a viscous torque between two neighbouring disk annuli at radius r

$$T_{\text{visc}} = 2\pi r \int dz\, r\tau = 2\pi \nu \Sigma r^3 \frac{d\Omega}{dr}, \tag{132}$$

where $\Sigma = \int dz\, \rho$ is the surface density of the disk (dependent on r). By employing the Keplerian orbital frequency it follows that the torque is

$$T_{\text{visc}} = -3\pi \nu \Sigma r^2 \Omega. \tag{133}$$

One may employ the α-disk prescription to parametrize the dynamical viscosity in the case for a thin accretion disk as $\nu = \alpha c_s^2 \Omega^{-1}$, where c_s is the gas sound speed (dependent on r) and $0 \leq \alpha \leq 1$ is a dimensionless constant ($\alpha = 0$ corresponds to no accretion). Substituting this expression for ν into the formula for T_{visc} gives

$$T_{\text{visc}} = -3\pi \alpha c_s^2 \Sigma r^2. \tag{134}$$

This torque results in an outward transfer of angular momentum and allows matter to accrete towards the central mass.

Continuity equation for accretion disks   Suppose that a gaseous disk has surface density $\Sigma(r)$. The structure and the evolution of gaseous disks can be deduced from the continuity equation

$$2\pi r \frac{\partial \Sigma}{\partial t} = \frac{\partial \dot{M}}{\partial r}, \tag{135}$$

and from angular momentum conservation

$$\frac{\partial (\Omega r^2)}{\partial r} \dot{M} = \frac{\partial}{\partial r}(T_{\text{visc}}). \tag{136}$$

The quantity $\dot{M}(r)$ is the mass flux through the disk at a radius r. Combining equations (135) and (136) gives an evolution equation for the surface density Σ

$$\frac{\partial \Sigma}{\partial t} = \frac{1}{2\pi r} \frac{\partial}{\partial r} \left[\left(\frac{\partial (\Omega r^2)}{\partial r} \right)^{-1} \frac{\partial (T_{\text{visc}})}{\partial r} \right]. \tag{137}$$

We can incorporate external effects acting onto the disk by modifying the viscous evolution equation of the disk: If the disk experiences an external torque per unit mass $\tilde{T}_{\text{ext}}$, the surface density evolution is modified according to

$$\begin{aligned}
\frac{\partial \Sigma}{\partial t} &= \frac{1}{2\pi r} \frac{\partial}{\partial r} \left[\left(\frac{\partial (\Omega r^2)}{\partial r} \right)^{-1} \frac{\partial (T_{\text{visc}})}{\partial r} + \frac{4\pi \Sigma \tilde{T}_{\text{ext}}}{\Omega} \right] \\
&= \frac{1}{2\pi r} \frac{\partial}{\partial r} \left[\left(\frac{\partial (\Omega r^2)}{\partial r} \right)^{-1} \frac{\partial (T_{\text{visc}} + T_{\text{ext}})}{\partial r} \right],
\end{aligned} \tag{138}$$

defining $\frac{\partial T_{\text{ext}}}{\partial r} = 8\pi \Sigma \tilde{T}_{\text{ext}} r$.

3.2 A model for the disk-binary interaction

Numerical simulations suggest the presence of a depleted cavity inside of which the binary resides. The gas orbiting around this cavity is referred to as the circumbinary disk (CBD). The evolution of the semi-major axis and of the orbital eccentricity are driven by tidal and viscous interactions between the binary and the CBD. We will set up a simplified and idealized model of this picture and see that the phenomena may result in a loss of the binary's orbital angular momentum, a increase in its eccentricity and its faster inspiral.

We thus now assume that the binary system has quickly excavates an inner cavity in the gas distribution and that the central cavity is surrounded by a circumbinary disk. Unfortunately, we don't know the timescale for formation of the cavity, because also the simulations already assume an initial cavity. For simplicity we also assume that neither the primary nor the secondary have their own disks. We aim to relate the viscous angular momentum flux in the inner region of the circumbinary disk to the orbital evolution of the binary.

The numerical simulations (see *e.g.* [16]) suggest that the size of the central cavity extends to about twice the semi-major axis of the binary orbit (as seen from the center of mass frame). This holds for binaries on circular orbits. Artymowicz & Lubow [17] showed through simulations that the location of the inner edge progresses outwards with increasing eccentricity, in their simulations from $r_{\rm in} \approx 1.9a$ for $e \approx 0.02$ to $r_{\rm in} \approx 3a$ for $e \approx 0.6$. These findings are also in accordance with simulations performed by Hayasaki *et al.* [18] where for $e = 0.5$ the inner edge was located at $r_{\rm in} \approx 2.8a$. Also, the above simulations suggest that the gap size seems to be approximately the same for different binary mass ratios q. Inspired by their findings, we thus estimate the inner edge of the circumbinary disk to be set by the twice the distance of the binary at apocenter, *i.e.* $r_{\rm in} = 2a(1 + e)$, and extrapolate this estimate also to eccentricities up to unity. This is not justified and it is likely that modifications occur for higher eccentricities. Towards more definite answers, one has to admit, there is no way around of performing hydrodynamical simulations. The simulations also show that the cavity is circular shaped, independent of the eccentricity of the binary orbit.

Tidal torques from the binary are expected to act significantly only on a narrow annulus at the inner edge of the CBD and are thus assumed to be zero outside of some cutoff radius r_Λ, which is very similar to $r_{\rm in}$. Thus the effect of the binary torque on the disk evolution can be accounted for via equation (138) by imposing suitable boundary conditions at the inner edge of the disk. From the previous subsection we deduce

$$\left(\frac{\partial(\Omega r^2)}{\partial r}\right)\dot{M} = \frac{\partial(T_{\rm visc})}{\partial r} + \left(\frac{\partial(\Omega r^2)}{\partial r}\right)\frac{4\pi\Sigma_g\tilde{T}_{\rm ext}}{\Omega}. \tag{139}$$

Integrating from r_b to r_Λ we obtain

$$T_{\rm visc}(r_\Lambda) = -8\pi\int_{r_b}^{r_\Lambda} dr\, r\Sigma_g\tilde{T}_{\rm ext} + 2\int_{r_b}^{r_\Lambda} dr\, r\Omega\dot{M}; \tag{140}$$

30

we have set $T_{\text{visc}}(r_b) = 0$ because of the clean gap assumption.

The first integral on the right hand side is the total torque the binary exerts on the disk, that is to say, the rate of the angular momentum injection into the disk by the binary. As long as the evolution of the binary is driven predominantly by the interaction with the disk, conservation of angular momentum guarantees that this term equals the change of angular momentum of the binary. In the right integral on the right side we can write

$$|\dot{M}| = 3\pi\Sigma_g\nu = 3\pi\Sigma_g\alpha c_s^2/\Omega. \tag{141}$$

Because of the clean gap assumption, the disk surface density Σ_g is zero for $r < r_{in}$. Thus we approximate the integral by

$$\begin{aligned}
\Delta &\equiv 6\pi\alpha c_s^2\Sigma_g(r_{in})\int_{r_{in}}^{r_\Lambda} dr\, r \\
&= 3\pi\alpha c_s^2\Sigma_g(r_{in})\left[r_\Lambda^2 - r_{in}^2\right] \\
&\approx 3\pi\alpha c_s^2\Sigma_g(r_{in})\delta r_{in},
\end{aligned}$$

where we set the disk density in the small radial annulus $[r_{\text{in}}, r_\Lambda]$ around the cavity edge to $\Sigma_g(r_{in})$ since $r_\Lambda - r_{\text{in}} = \delta/2 \ll r_{\text{in}}$ and since we have no model to resolve the surface density of the CBD down to this scale.

From here forward, we will work in the reference frame of the binary system. The binary injects angular momentum into the disk, so we require $\dot{L}_b < 0$. According to this convention, in the binary reference frame the sign of the viscous torque must be opposite to that of equation (134). Thus the viscous torque reads $T_{\text{visc}}(2a(1+e)) = 12\pi\alpha c_s^2\Sigma_g a^2(1+e)^2$. Here c_s and Σ_g are to be evaluated at r_{in} (however, towards the end of this section we will have abandoned the hope to actually model the profile of the CBD). As $T_{\text{visc}}(2a(1+e))$ is a few order of magnitudes higher than Δ, we neglect Δ henceforth. In the binary frame, equation (140) therefore translates into

$$T_{\text{visc}}(r_{\text{in}}) = -\dot{L}_b. \tag{142}$$

We impose a further assumption to the particular evolution model, namely that the binary-disk interaction may well be approximated as an adiabatic process (as opposed to an evolution that is driven by sudden perturbations, like the gravitational wave capture scenario of section 2.3). In other words, we assume that the timescale of the disk-binary interaction is much larger than some characteristic timescale of the binary, like its orbital period. It has to emphasized that this is an idealized assumption; it is somewhat supported by the simulations because they show the maintenance of the circular shape of the cavity across a large spectrum of eccentricities (see section (3.2.1) for a broader analysis of this argument). Under the adiabatic assumption, the change in the binary energy can be related to its change in angular momentum through the orbital frequency,

$$\dot{E}_b = \Omega_b\dot{L}_b. \tag{143}$$

Note that $\dot{L}_b < 0$, so $\dot{E}_b < 0$ and therefore the binary system always evolves toward lower energy. In particular an initially bound orbit always stays on

an elliptic orbit. Energy conservation implies that energy is deposited in the circumbinary disk and this dissipated energy may *e.g.* heat up the disk material. From the evolution equation (11) for the semi-major axis of the binary orbit and the binary energy $E_b = -\frac{\Omega_b L_b}{2\sqrt{1-e^2}}$ it follows that

$$\frac{\dot{a}}{a} = -\frac{\dot{E}_b}{E_b} = -\frac{T_{\text{visc}}(r_{\text{in}})}{L_b} 2\sqrt{1-e^2} \tag{144}$$

$$= -2\frac{T_{\text{visc}}(r_{\text{in}})}{\mu\Omega_b a^2}, \tag{145}$$

where the last equation follows by substituting the orbital angular momentum (9). Substituting the explicit formula for the viscous torque results in

$$\dot{a} = -\frac{24\pi a\alpha c_s^2 \Sigma_g (1+e)^2}{\mu\Omega_b}. \tag{146}$$

Starting from the standard evolution equation (12), we similarly get for the evolution of the eccentricity the expression

$$\dot{e} = \frac{1-e^2}{e}\left(\frac{1}{\sqrt{1-e^2}} - 1\right)\frac{T_{\text{visc}}(r_{\text{in}})}{\mu\Omega_b a^2} \tag{147}$$

$$= \frac{(1+e)^2}{e}(\sqrt{1-e^2} + e^2 - 1)\frac{12\pi\alpha c_s^2 \Sigma_g}{\mu\Omega_b}. \tag{148}$$

Inspection of the evolution equations shows that in this model for $a \neq 0$ the semi-major axis decreases in time and the orbital eccentricity doesn't change for $e = 0$ and increases in time for $e \neq 0$. Even though we have $\dot{e} \geq 0$, the orbit cannot become unbound since the orbit's energy is decreasing. In effect, the disk-binary dynamics will drive the binary into a regime where gravitational wave emissions will dominate the orbital evolution.

We can divide equation (146) by equation (148) and solve the resulting differential equation. We get

$$a(e) = a_0 \left(\frac{1 - \sqrt{1-e_0^2}}{1 - \sqrt{1-e^2}}\right)^2, \tag{149}$$

with initial semi-major axis a_0 and initial eccentricity e_0. But as indicated above, it would not be meaningful to assert that the disk dynamics alone can provide a full description of the orbital evolution.

In chapter (4) we need to insert values for α, Σ_g, c_s and h/r of the CBD. We set those quantities of the circumbinary disk equal to those of the background disk at the location where the binary resides within the background disk. One may argue that the quantities taken at the inner edge of the CBD should not differ significantly from the quantities taken at the outer edge of the CBD and there those quantities should not differ from their values in the background disk. The inspiration for using this assumption comes from Baruteau *et al.* [19], who use exactly the same assumption for the same problem. We realize that this assumption is not satisfactory, but due to the lack of a better alternative we will use it.

3.2.1 Shortcomings of the model

The implicit assumption on the disk-binary interaction than goes along by employing equation (143) may be phrased in another way. Namely, that the non-axisymmetric potential perturbations of the binary system are assumed to be small around the average binary potential. This is certainly fulfilled for circular orbits and also for orbits with low eccentricity. For higher eccentricities there is no good reason why this assumption should hold. But since the hydrodynamical simulations do not show signs of non-circular cavity shapes even for large eccentricities, we assume the torque to act on average axially-symmetrically onto the disk.

Along the same lines, the use of assumption (143) really reflects our ignorance of the character of the energy flux between the binary and the disk. For a deeper understanding of the energy flux one needs a microscopic understanding of the disk-binary interaction that does not rely on a macroscopic orbital averaging of dynamical parameters. At the level of Hamiltonian dynamics, we assume in this evolution channel that the Hamiltonian describing the disk-binary interaction only depends on the angular momentum of the binary. For a more refined and correct treatment of the problem it is necessary to also include the position and momentum coordinates of the binary into the Hamiltonian.

3.3 Results from the binary evolution channel

From this section onwards, all equations, plots and numerical values are expressed in SI units.

Both gravitational wave emission and the disk interaction affect the evolution of the binary system. To investigate the dynamics of the interplay between both effects, we combine $\dot{a}_{\text{disk-binary}}$ (expression 146)) and $\dot{e}_{\text{disk-binary}}$ (expression 148)) of the disk-driven orbital evolution channel with the corresponding gravitational wave driven evolution equations $\dot{a}_{\text{GW}}$ and $\dot{e}_{\text{GW}}$ of section (2.4). The combined dynamics is thus described by the evolution equations

$$
\begin{aligned}
\dot{a} &= \dot{a}_{\text{GW}} + \dot{a}_{\text{disk-binary}}, \\
\dot{e} &= \dot{e}_{\text{GW}} + \dot{e}_{\text{disk-binary}}.
\end{aligned}
\tag{150}
$$

We integrate this coupled system of differential equations numerically. Among the various ordinary differential equations solvers in Matlab, the ode23tb function performed best. This solver is designed for solving stiff ordinary differential equations. That the evolution equations exhibit stiffness is not too surprising; during the latest stages of inspiral, the solution does indeed display much variation within a short time interval.

The numerical integration yields the temporal evolution of the semi-major axis and the eccentricity that results from the particular evolution channel (150). Of particular interest is the time to merger of a binary system with orbital parameters M and μ, initial conditions a_0 and e_0 and that is embedded in a CBD with disk parameters Σ, c_s, α and aspect ratio h/r (recall from the previous subsection the assumption that relates those quantities to the corresponding ones

of the background disk). The merger time is taken as the abscissa where the numerical solution $a(t)$, or $e(t)$, approaches the abscissa axis.

At most values of the semi-major axis a the disk-binary interaction dominates the gravitational wave emission. Only at the latest stages of inspiral when a is sufficiently low, gravitational emission becomes important. The combined evolution reduces the purely gravitational wave-driven merger time by several orders of magnitudes. Binary systems with a certain configuration of orbital parameters that are not embedded into a disk would not merge within a Hubble time, which is about 1.4×10^{10} years. A gaseous environment would provide a mechanism for such binaries to merge. Let us illustrate the above assertion by an example. Figure (3) shows, as a function of the orbit's initial eccentricity, the purely gravitational wave-driven merger times (blue) and those where in addition disk interactions are taken into account (green). For the disk parameters we used $M_{\mathrm{SMBH}} = 1 \times 10^7 M_\odot, \alpha = 0.1, f_g = 0.1$ and $h/r = 0.01$. The binary's location in the disk is $r = 0.1$ pc and we have set $M = 50 M_\odot, \mu = M/4, a_0 = 1$ AU. The merger time for $e = 0.01$ premised upon the disk-GW channel is 1.76×10^8 years (compared to 1.01×10^{13} years for the purely GW driven evolution), for $e = 0.99$ it is 1.97×10^5 years (as opposed to 1.69×10^7 years for the purely GW driven evolution). Of course, if the initial semi-major axis a_0 is already sufficiently low, then the orbit evolves only due to gravitational radiation and the disk interaction has no imprint on the orbital evolution. Using as an illustration the disk parameters of the previous example and an initial eccentricity of $e_0 = 0.3$, then for $a_0 < 0.02$ AU the disk interaction plays no dominant role in the orbital evolution (at $a_0 = 0.02$ AU, the merger time is 1.13×10^6 years).
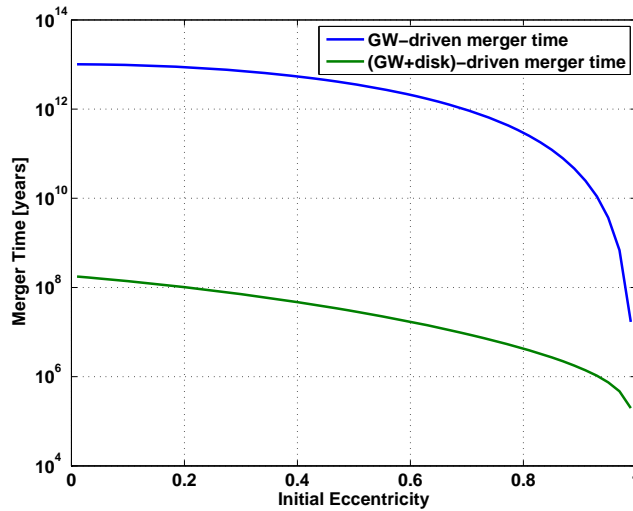
Figure 3: Merger times as a function of the initial binary eccentricity. The blue curve represents the merger times resulting from GW-driven decay, the green one resulting from both GW emission and disk-binary interaction.

The disk-binary dynamics reduces the elliptic binary's semi-major axis while at the same time it increases the elliptic orbit's eccentricity. At a critical semi-major axis, where $\dot{a}_{\mathrm{GW}} = \dot{a}_{\mathrm{disk\text{-}binary}}$, the binary evolution changes from being

predominately disk driven to being predominately driven by gravitational wave emission. Here is again a numerical illustration. Figure (4) displays the orbit's semi-major axis as a function of the orbit's eccentricity for initial eccentricities e_0 ranging from 0.01 to 0.9. The black circles indicate the transition where $\dot{a}_{\mathrm{GW}}$ starts dominating over $\dot{a}_{\mathrm{disk\text{-}binary}}$. The parameters of the binary are $a_0 = 1$ AU, $M = 50 M_\odot$ and $q = 1$. The binary system is located at $r = 0.1$ pc in a disk with characteristics $M_{\mathrm{SMBH}} = 1 \times 10^7 M_\odot, \alpha = 0.1, f_g = 0.1$ and $h/r = 0.01$. From the figure we also observe that the eccentricity at the transition semi-major axis does not necessarily coincide with the maximum eccentricity reached during the entire orbital evolution. This is because $\dot{a}_{\mathrm{GW}} = \dot{a}_{\mathrm{disk\text{-}binary}}$ doesn't necessarily imply $|\dot{e}_{\mathrm{GW}}| = |\dot{e}_{\mathrm{disk\text{-}binary}}|$.
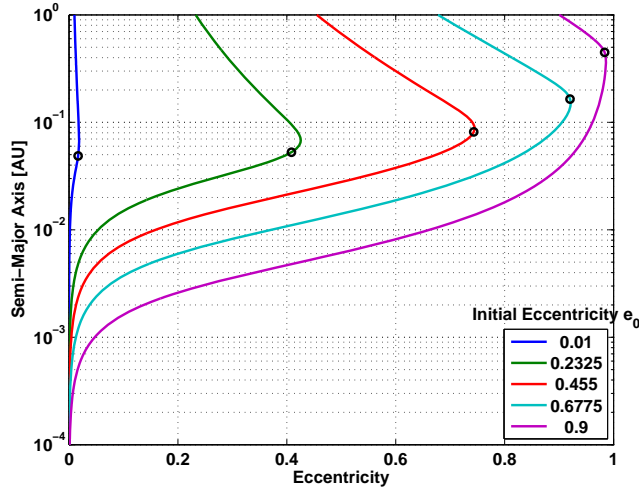

Figure 4: The orbital semi-major axis as a function of the orbit's eccentricity for a binary systems premised on the evolution equations (150). In this plot we show $a(e)$ for different initial eccentricities. The disk-binary interaction decreases the orbit's semi-major axis and increases the orbit's eccentricity. The last stages of the orbital evolution are driven by gravitational wave emission and this causes the merging of the binary.

In figure (5) we plot the orbital decay rate $\dot{a}$ along the semi-major axis a for a binary and a disk that have the same configuration as in figure (4). At initially large values of the semi-major axis, the rate $\dot{a}_{\mathrm{disk\text{-}binary}}$ dominates over $\dot{a}_{\mathrm{GW}}$. In the purely disk-driven regime we find from equations (146) and (149) that the semi-major axis evolves as

$$\dot{a}_{\mathrm{disk\text{-}binary}} \propto -a^{5/2} \left(1 + a^{-1/4} \right)^2. \tag{151}$$

Only at sufficiently small semi-major axis the gravitational wave emission starts governing the orbital decay. The black circles in figure (5) show again the transition where $\dot{a}_{\mathrm{GW}}$ starts dominating over $\dot{a}_{\mathrm{disk\text{-}binary}}$. The explicit expression for the dependence of the orbital decay rate on the semi-major axis in the gravitational wave driven regime is complicated, but can be extracted by inserting the

inverse of equation (122) into (119). We see from figure (4) that when the semi-major axis has reached $a \sim 10^3 - 10^{-4}$ AU, the orbit has nearly circularized. Therefore during and after this regime the slope of the orbital decay is

$$\dot{a}_{\mathrm{GW}} \propto -a^{-3}. \tag{152}$$
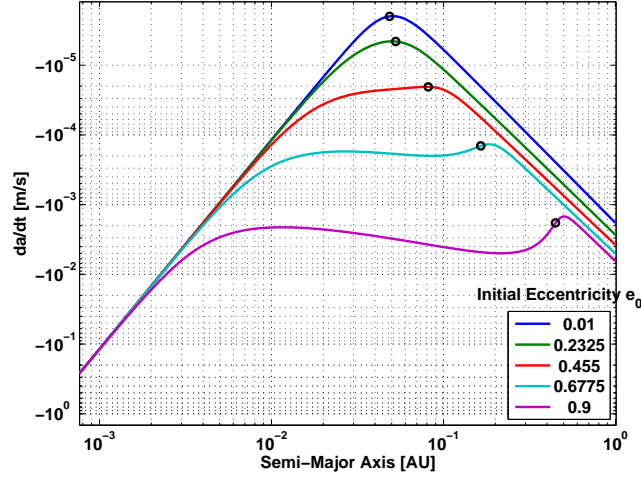
Figure 5: Davsa: Left,small a: GW slope, right: Disk slope

In this binary evolution model, the primary cause for the faster coalescence as compared to the purely gravitational wave evolution channel is the eccentricity growth that the binary experiences due to the disk-interaction. The maximal eccentricity $e_{\max}$ that is reached during the binary evolution increases as e_0 and a_0 increase and decreases as M and q increase. These dependencies reflect themselves also in the merger time dependence: The higher e_0 and a_0, the faster the coalescence and the higher M and q, the longer it takes the binary to merge. These dependencies can be seen from . In contrast, for an orbital evolution purely driven by gravitational waves the merger time decreases as e_0, M and q increase and increases as a_0 increase. Table (1) gives once more numerical examples. There we list $e_{\max}$, $a(e_{\max})$ and the merger time for binary systems where only a selected binary parameter is varied. Higher initial eccentricities lead to higher $a(e_{\max})$ and to a faster coalescence.

		e_{max}	$a(e_{\mathrm{max}})$ [AU]	Merger time [years]
Initial eccentricity	$e_0 = 0.01$	0.02	0.07	1.76×10^8
	$e_0 = 0.9$	0.98	0.36	1.58×10^6
Initial semi-major axis	$a_0 = 1$ AU	0.54	0.07	7.07×10^7
	$a_0 = 20$ AU	0.88	0.12	1.69×10^7
Binary Mass	$M = 10\,M_\odot$	0.69	0.02	2.91×10^7
	$M = 100\,M_\odot$	0.47	0.12	9.72×10^7
Mass ratio	$q = 0.05$	0.61	0.04	2.71×10^7
	$q = 1$	0.54	0.07	7.08×10^7

Table 1: Parameter study.

4 Merger rate density estimation

In this section we want to investigate the binary black hole (BBH) merger rate density that could be expected from the binary evolution channel of the previous chapter. The merger rate density we take as the number of coalescences per unit time per unit volume.

In McKernan *et al.* [20] the merger rate density of black hole binary mergers in AGN disks is parametrized as

$$\mathcal{R}_{\mathrm{McK}} = \frac{N_{\mathrm{BHs}}\, f_b\, f_d\, n_{\mathrm{AGN}}}{\tau_{\mathrm{avg}}}. \tag{153}$$

Here N_{BHs} is the number of stellar mass black holes per galactic nucleus, f_b is the fraction of black holes residing within binaries, f_d is the fraction of black holes embedded in the AGN disk (that is, $N_{\mathrm{BHs}}f_b f_d/2$ is the number of binary black holes embedded in the disk), n_{AGN} is the number density of active galactic nuclei and τ_{avg} is the average binary merger time. In McKernan *et al.* the prescription (153) is taken as a starting point, however, no attempt is then made to estimate the average merger time of binary systems (it is instead assumed that all binaries merge within the lifetime of the disk). All the same, the prescription (153) is unsatisfactory for a different reason: Resorting to an average time scale when determining rates underestimates BBH mergers with merger times smaller than τ_{avg} and overestimates BBHs with merger times higher than τ_{avg}.

We will determine the merger rate density from a weighted average of a population of BBH, in a sense made precise in sections (4.2) and (4.3).

4.1 Mass distributions

We will combine different mass distributions and mass density profiles to derive an expression for the number of black holes with a given mass range that reside within a radial shell of an AGN disk.

Stellar distribution We start with an initial stellar population. The initial stellar mass distribution seems to follow a multiple power-law function. Here we adopt the initial stellar mass function of Kroupa [21]

$$f_{\mathrm{IMF}}(m) = \begin{cases} k_0 \left(\frac{m}{M_\odot}\right)^{-0.3} & \text{if } m < 0.08 M_\odot \\ k_1 \left(\frac{m}{M_\odot}\right)^{-1.3} & \text{if } 0.08 M_\odot < m < 0.5 M_\odot \ , \\ k_2 \left(\frac{m}{M_\odot}\right)^{-2.3} & \text{if } m > 0.5 M_\odot \end{cases} \tag{154}$$

where the normalization parameters $k_0, k_1 = 0.08 k_0$ and $k_2 = 0.04 k_0$ are fixed by requiring the mass function to be continuous (see also Maschberger [22]). We assume that the lowest mass of the stars $m_{\mathrm{s,min}}$ is smaller than $0.08 M_\odot$ and that the highest mass $m_{\mathrm{s,max}}$ is above $0.5 M_\odot$. The normalization of the initial

mass function is taken such that $N_* = \int_{m_{\mathrm{s,min}}}^{m_{\mathrm{s,max}}} dm\, f_{\mathrm{IMF}}(m)$ and accordingly the parameter k_0 is

$$k_0 = \frac{N_*}{M_\odot} \Bigg/ \left[0.56 - \frac{1}{0.7} \left(\frac{m_{\mathrm{s,min}}}{M_\odot} \right)^{0.7} - \frac{0.04}{1.3} \left(\frac{m_{\mathrm{s,max}}}{M_\odot} \right)^{-1.3} \right]. \tag{155}$$

The total stellar mass is

$$M_* = \int_{m_{\mathrm{s,min}}}^{m_{\mathrm{s,max}}} dm\, m f_{\mathrm{IMF}} \tag{156}$$

$$= k_0 M_\odot^2 \left[0.22 - \frac{1}{1.7} \left(\frac{m_{\mathrm{s,min}}}{M_\odot} \right)^{1.7} - \frac{0.04}{0.3} \left(\frac{m_{\mathrm{s,max}}}{M_\odot} \right)^{-0.3} \right]. \tag{157}$$

We adopt the "Nuker law" parametrization ([23]) for the stellar density profile $\rho_*(r)$

$$\rho_*(r) \propto \left(\frac{r_b}{r} \right)^\gamma \left[1 + \left(\frac{r}{r_b} \right)^\alpha \right]^{\frac{\gamma - \beta}{\alpha}}, \tag{158}$$

We simplify this profile by using its asymptomatic slopes,

$$\rho_*(r) = \begin{cases} \rho_0 \left(\frac{r}{r_b} \right)^{-\gamma} & \text{if } r \leq r_b \\ \rho_0 \left(\frac{r}{r_b} \right)^{-\beta} & \text{if } r > r_b \end{cases}; \tag{159}$$

the parameter α would parameterize the transition between the inner cusp and the outer power law. The break radius r_b is approximately on the order of the radius of influence of the SMBH ([24]), characterized as $r_b = M_{\mathrm{SMBH}}/\sigma^2$ (σ is the stellar dispersion). The normalization parameter ρ_0 can then be expressed as

$$\rho_0 = \frac{M_*}{4\pi r_b^3} \left(\frac{1}{3 - \gamma} - \frac{1}{3 - \beta} \right)^{-1}, \tag{160}$$

where we further included the assumption that we only consider models with $\beta > 3$.

BH distribution If we assume that every star heavier than $m_{\mathrm{s,cr}} \sim 5 M_\odot$ evolved into a BH, the total number of BHs is

$$N_{\mathrm{BHs}} = \int_{m_{\mathrm{s,cr}}}^{m_{\mathrm{s,max}}} dm\, f_{\mathrm{IMF}}$$

$$= -\frac{0.04}{1.3} k_0 M_\odot \left[\left(\frac{m_{\mathrm{s,max}}}{M_\odot} \right)^{-1.3} - \left(\frac{m_{\mathrm{s,cr}}}{M_\odot} \right)^{-1.3} \right] \tag{161}$$

$$= k M_*,$$

where we defined

$$k = \frac{1}{M_\odot} \frac{-\frac{0.04}{1.3} \left[\left(\frac{m_{\mathrm{s,max}}}{M_\odot} \right)^{-1.3} - \left(\frac{m_{\mathrm{s,cr}}}{M_\odot} \right)^{-1.3} \right]}{\left[0.22 - \frac{1}{1.7} \left(\frac{m_{\mathrm{s,min}}}{M_\odot} \right)^{1.7} - \frac{0.04}{0.3} \left(\frac{m_{\mathrm{s,max}}}{M_\odot} \right)^{-0.3} \right]}. \tag{162}$$

The total mass of all BHs is

$$M_{\mathrm{BH}} = \int_{m_{\mathrm{s,cr}}}^{m_{\mathrm{s,max}}} dm\, m\, f_{\mathrm{IMF}}. \tag{163}$$

The BH mass distribution is denoted as $f_{\mathrm{BH}}(m)$ and is normalized such that $\int dm f_{\mathrm{BH}}(m) = 1$. We adopt a Salpeter mass function for the BH distribution

$$f_{\mathrm{BH}}(m) = \xi_0 m^{-2.35}; \tag{164}$$

the normalization parameter ξ_0 is accordingly

$$\xi_0 = -\frac{1.35}{m_{\mathrm{BH,max}}^{-1.35} - m_{\mathrm{BH,min}}^{-1.35}}. \tag{165}$$

If $N(r)$ denotes the total number of BHs inside some radius r, the number dN of BHs lying inside r with masses between m and $m + dm$ is

$$dN = N(r) f_{\mathrm{BH}}(m) dm \tag{166}$$
$$= k M_*(r) f_{\mathrm{BH}}(m) dm, \tag{167}$$

where $M_*(r)$ is the total stellar mass inside radius r ($M_*(\infty) \equiv M_*$). Note that for the last equality we assumed that the mass distribution of the BHs is independent of the radius at which they reside (an assumption that could be refined, but it is used in the literature, see $e.g$ [25]). We can write dN in the following form

$$dN = dm\, k\, f_{\mathrm{BH}}(m) \int_0^r dr\, \rho_*(r) 4\pi r^2, \tag{168}$$

and this yields finally

$$\frac{dN}{dm} = \begin{cases} k\, f_{\mathrm{BH}}(m) \frac{4\pi\rho_0}{3-\gamma} r_b^\gamma r^{3-\gamma} & \text{if } r \leq r_b \\ k\, f_{\mathrm{BH}}(m) 4\pi\rho_0 r_b^3 \left[\frac{1}{3-\gamma} + \frac{1}{3-\beta} \left[\left(\frac{r}{r_b}\right)^{3-\beta} - 1 \right] \right] & \text{if } r > r_b \end{cases}. \tag{169}$$

The number of BHs with masses between m and $m + dm$ in a radial shell from radius r to $r + dr$ is accordingly

$$\begin{cases} dm\, k\, f_{\mathrm{BH}}(m) \frac{4\pi\rho_0}{3-\gamma} r_b^\gamma \left[(r+dr)^{3-\gamma} - r^{3-\gamma} \right] & \text{if } r \leq r_b \\ dm\, k\, f_{\mathrm{BH}}(m) \frac{4\pi\rho_0}{3-\beta} r_b^3 \left[\left(\frac{r+dr}{r_b}\right)^{3-\beta} - \left(\frac{r}{r_b}\right)^{3-\beta} \right] & \text{if } r > r_b \end{cases}. \tag{170}$$

The total number of BHs in a radial shell from radius r to $r + dr$ is

$$\begin{cases} k \frac{4\pi\rho_0}{3-\gamma} r_b^\gamma \left[(r+dr)^{3-\gamma} - r^{3-\gamma} \right] & \text{if } r \leq r_b \\ k \frac{4\pi\rho_0}{3-\beta} r_b^3 \left[\left(\frac{r+dr}{r_b}\right)^{3-\beta} - \left(\frac{r}{r_b}\right)^{3-\beta} \right] & \text{if } r > r_b \end{cases}. \tag{171}$$

4.2 Rate per galactic nucleus

To estimate the merger rate per galactic nucleus, we add up the rate contributions coming from different radial shells. We assume that the AGN disk

around the supermassive black hole extends from $r_{\min}$ to $r_{\max}$. We partition the disk into $\mathcal{I}_r$ intervals . The number of BHs within each radial shell $[r_{\min} + j\Delta r, r_{\min} + (j+1)\Delta r]$, where $\Delta r = (r_{\max} - r_{\min})/|\mathcal{I}_r|$, is obtained from equation (171)

$$
N_j = \begin{cases} k\,\frac{4\pi\rho_0}{3-\gamma} r_b^\gamma \left[(r_{\min} + (j+1)\Delta r)^{3-\gamma} - (r_{\min} + j\Delta r)^{3-\gamma} \right] & \text{if } r_{\min} + (j+1)\Delta r \le r_b \\ k\,\frac{4\pi\rho_0}{3-\beta} r_b^3 \left[\left(\frac{r_{\min}+(j+1)\Delta r}{r_b}\right)^{3-\beta} - \left(\frac{r_{\min}+j\Delta r}{r_b}\right)^{3-\beta} \right] & \text{if } r_{\min} + j\Delta r > r_b \end{cases}
$$

$$(172)$$

The mean radius of a radial shell is

$$r_j = r_{\min} + (j + 0.5)\Delta r. \tag{173}$$

The number of BBHs within each radial shell that are embedded in the disk is given by

$$N_{\mathrm{BBH},j} = \frac{N_j f_b f_d}{2}. \tag{174}$$

4.2.1 BBH distributions in a radial shell

Within each radial shell labelled by j we distribute the number of BBHs $N_{\mathrm{BBH},j}$ for the binary parameter $(m_1, m_2, e_0, a_0) \cong (m_1 \equiv \tilde{M}, q, e_0, a_0)$ according to some canonical binary parameter distribution functions. We assume for simplicity that the binary parameter distributions are independent from each other. The distributions in this subsection are normalized with respect to the total number of BBHs $N_{\mathrm{BBH},j}$ in a single radial shell $[r_{\min} + j\Delta r, r_{\min} + (j+1)\Delta r]$.

Primary mass distribution   We adopt the initial mass function of Salpeter for the primary mass distribution. Thus, in a radial shell $[r_{\min} + j\Delta r, r_{\min} + (j+1)\Delta r]$, the number of binaries with primary mass between m and $m + dm$ is given by

$$2\pi f_b f_d dm\, k\, f_{\mathrm{BH}}(m)\,\rho_0$$
$$\times \begin{cases} \frac{1}{3-\gamma} r_b^\gamma \left[(r_{\min} + (j+1)\Delta r)^{3-\gamma} - (r_{\min} + j\Delta r)^{3-\gamma} \right] & \text{if } r_{\min} + (j+1)\Delta r \le r_b \\ \frac{1}{3-\beta} r_b^3 \left[\left(\frac{r_{\min}+(j+1)\Delta r}{r_b}\right)^{3-\beta} - \left(\frac{r_{\min}+j\Delta r}{r_b}\right)^{3-\beta} \right] & \text{if } r_{\min} + j\Delta r > r_b \end{cases}$$

$$(175)$$

Secondary mass distribution   The secondary mass distribution is determined by the distribution of the mass ratio q, assumed to follow a uniform distribution (see Tout *et al.* [26] or Ablimit & Maeda [27])

$$f(q) = \vartheta_0, \tag{176}$$

where ϑ_0 is a constant and $q_{\min} \le q \le q_{\max}$. From the normalization condition $\vartheta_0 \int_{q_{\min}}^{q_{\max}} dq = N_{\mathrm{BBH},j}$ we extract $\vartheta_0 = N_{\mathrm{BBH},j}/(q_{\max} - q_{\min})$.

Orbital separation distribution   The distribution of the initial orbital separation a_0 is assumed to be logarithmically flat (see again [26],[27])

$$f(a_0) = \chi_0/a_0, \tag{177}$$

between the limits $a_{0,\min}$ and $a_{0,\max}$. From the normalization with respect to $N_{\mathrm{BBH},j}$ we obtain $\chi_0 = N_{\mathrm{BBH},j} \big/ \log\left(\frac{a_{0,\max}}{a_{0,\min}}\right)$.

Orbital eccentricity distribution   We choose the distribution of the initial orbital eccentricity e_0 to follow a thermal distribution (see [26])

$$f(e_0) = \varsigma_0 e_0, \tag{178}$$

between the limits $e_{0,\min}$ and $e_{0,\max}$. The number of BBHs below a given eccentricity e scale in a thermal distribution as e^2. The normalization with respect to $N_{\mathrm{BBH},j}$ gives $\varsigma_0 = 2N_{\mathrm{BBH},j} \big/ \left(e_{0,\max}^2 - e_{0,\min}^2\right)$.

4.2.2   Calculation of rate within a radial shell

We have set up everything to finally perform the calculation of the rate of coalescences in a radial shell. To this end, we partition each binary parameter into bins and distribute $N_{\mathrm{BBH},j}$, the total number of BBHs within a shell, among the different bins. The merger rate is then ascertained as follows:

The sets $\mathcal{I}_x$ (where x is one of $\tilde{M}, q, e_0$ or a_0) will denote the number of bins for the corresponding binary distributions x. The numbers $N_{x,i}$ will denote the number of BBHs residing within the bin $i \in \mathcal{I}_x$ of the binary distribution x. We need to take all possible combinations of the bins $\mathcal{I}_{\tilde{M}}$, $\mathcal{I}_q$, $\mathcal{I}_{a_0}$ and $\mathcal{I}_{e_0}$ and calculate for each such combination the binary's merger time based on the evolution equations (150). We denote such a combination by $\lambda \in \mathcal{I}_{\tilde{M}} \times \mathcal{I}_q \times \mathcal{I}_{a_0} \times \mathcal{I}_{e_0}$ and the merger time corresponding to this combination by $\tau_{\mathrm{merger},\lambda}$. We take as the input values needed for the numerical calculation of the merger time the average quantities x_i of the orbital parameter x in bin i. The total number of BBHs inhabiting a combination $\lambda = (k,l,u,v)$ is given by $N_{\tilde{M},k} N_{q,l} N_{a_0,u} N_{e_0,v} / N_{\mathrm{BBH},j}^3 \equiv N_\lambda / N_{\mathrm{BBH},j}^3$. The total merger rate resulting from a radial shell labelled by j is therefore

$$\mathcal{R}_j = \sum_\lambda \frac{N_\lambda}{N_{\mathrm{BBH},j}^3} \frac{1}{\tau_{\mathrm{merger},\lambda}}, \tag{179}$$

where the sum goes over all $\lambda \in \mathcal{I}_{\tilde{M}} \times \mathcal{I}_q \times \mathcal{I}_{a_0} \times \mathcal{I}_{e_0}$.

The number $N_{x,i}$ of BBHs inside a bin $i \in \mathcal{I}_x$ of the binary parameter x and the average of x within this bin are straightforward but awkward to write down. We put those expressions into appendix (7.2).

Let's elucidate again what parameters enter in the calculation of the merger time $\tau_{\mathrm{merger},\lambda}$ for a bin combination $\lambda = (k,l,u,v)$. The binary system itself is characterized by its primary mass $\tilde{M}_k$ and its mass ratio q_l. The initial conditions to solve the evolution equations (150) are the initial orbit's semi-major axis a_{0_u} and the initial orbit's eccentricity e_{0_v}. The viscosity parameter, the aspect ratio, the surface density and the gas density fraction of the CBD are inferred from the corresponding values of the AGN disk, the latter two evaluated at the radius r_j. The numbers $N_{\mathrm{BBH},j}$ and $N_{x,i}$ depend on $f_b, f_d, m_{s,\mathrm{cr}}, m_{\mathrm{BH,min}}, m_{\mathrm{BH,max}}, m_{s,\min}, m_{s,\max}, N_*, M_{\mathrm{SMBH}}, \gamma, \beta$.

4.2.3 Merger rate for a galactic nucleus

The merger rate for a galactic nucleus is obtained by summing up the rate (179) for each radial shell,

$$\mathcal{R}_{\text{gal}} = \sum_{j \in \mathcal{I}_r} \mathcal{R}_j. \tag{180}$$

4.3 Merger rate density

The merger rate density $\mathcal{R}$ is given by

$$\mathcal{R} = \mathcal{R}_{\text{gal}} \, n_{\text{AGN}}. \tag{181}$$

The number N_* of stars within r_{max}, the fraction f_b of BH in BBHs, the fraction f_d of BHs embedded in the disk and the number density n_{AGN} of active galactic nuclei affect the merger rate density $\mathcal{R}$ only as scaling factors. For this reason we will report rate densities in a form where we have set those scaling factors to a fixed value. To be specific, for f_b, f_d and n_{AGN} we adopt the population parameters (in parenthesis we indicate the lower bound and upper limits) from McKernan *et al.* [20]

- $\diamond$ The fraction f_b of BH in BBH we estimate as 0.1 $[0.01, 0.2]$

- $\diamond$ The fraction f_d of BH embedded in the disk we estimate as 0.01 $[0.01, 0.7]$

- $\diamond$ The number density n_{AGN} of active galactic nuclei we estimate as 4×10^4 Gpc^{-3} $[4 \times 10^4$ Gpc^{-3}, 3×10^6 Gpc$^{-3}]$

In addition we fix $r_{\text{max}} = 1$ pc. The inner edge of the accretion disk can in principle go down to about a few Schwarzschildradii, but we don't expect binaries to reside there. So we set fiducially r_{min} to 100 times the Schwarzschilradius. The number N_* of stars residing within 1 pc we estimate as 1×10^6. Furthermore, we use the fiducial values $m_{\text{s,min}} = 0.01 M_\odot, m_{\text{s,max}} = 200 M_\odot$ and $m_{\text{s,cr}} = 5 M_\odot$. The number of BH within 1 pc, obtained from formula 161, is then about 7.5×10^3, a value in accordance with the lower bound 10^3 and upper bound 10^6 adopted in McKernan *et al.*.

Additionally we use the fiducial values $\beta = 3.2$ and $\gamma = 1.5$ for the mass distribution parameters. Also we adopt throughout a disk aspect ratio $h/r = 0.01$, a gas fraction $f_g = 0.1$ and a viscosity parameter $\alpha = 0.1$.

$r_{\rm min}$	9.63×10^{-4} pc	9.63×10^{-4} pc	9.63×10^{-4} pc
$[m_{\rm BH,min}, m_{\rm BH,max}]$	$[5, 50] \, M_\odot$	$[5, 50] \, M_\odot$	$[5, 50] \, M_\odot$
$[q_{\rm min}, q_{\rm max}]$	$[0.01, 1]$	$[0.01, 1]$	$[0.01, 1]$
$[a_{0,\rm min}, a_{0,\rm max}]$	$[0.1, 100]$ AU	$[0.1, 100]$ AU	$[0.1, 100]$ AU
$[e_{0,\rm min}, e_{0,\rm max}]$	$[0.001, 0.95]$	$[0.001, 0.95]$	$[0.001, 0.95]$
$M_{\rm SMBH}$	$1 \times 10^8 M_\odot$	$1 \times 10^8 M_\odot$	$1 \times 10^8 M_\odot$
$\mathcal{I}_{r,\tilde{M},q,a_0,e_0}$	$(20, 10, 10, 10, 20)$	$(15, 15, 15, 15, 15)$	$(20, 20, 20, 20, 20)$
$\tau_{\rm avg}$ [years]	1.83×10^7	1.78×10^7	1.81×10^7
$\tau_{\rm med}$ [years]	3.35×10^5	3.22×10^5	3.15×10^5
$\mathcal{R}$ [year^{-1} Gpc^{-3}]	0.40	0.36	0.45

$r_{\rm min}$	9.63×10^{-6} pc	9.63×10^{-5} pc	9.63×10^{-4} pc
$[m_{\rm BH,min}, m_{\rm BH,max}]$	$[5, 50] \, M_\odot$	$[5, 50] \, M_\odot$	$[5, 50] \, M_\odot$
$[q_{\rm min}, q_{\rm max}]$	$[0.01, 1]$	$[0.01, 1]$	$[0.01, 1]$
$[a_{0,\rm min}, a_{0,\rm max}]$	$[0.1, 100]$ AU	$[0.1, 100]$ AU	$[0.1, 100]$ AU
$[e_{0,\rm min}, e_{0,\rm max}]$	$[0.001, 0.99]$	$[0.001, 0.99]$	$[0.001, 0.99]$
$M_{\rm SMBH}$	$1 \times 10^6 M_\odot$	$1 \times 10^7 M_\odot$	$1 \times 10^8 M_\odot$
$\mathcal{I}_{r,\tilde{M},q,a_0,e_0}$	$(20, 10, 10, 10, 20)$	$(20, 10, 10, 10, 20)$	$(20, 10, 10, 10, 20)$
$\tau_{\rm avg}$ [years]	3.12×10^9	2.34×10^8	1.75×10^7
$\tau_{\rm med}$ [years]	1.59×10^8	6.61×10^6	2.58×10^5
$\mathcal{R}$ [year^{-1} Gpc^{-3}]	3.9×10^{-2}	0.17	0.72

$r_{\min}$	9.63×10^{-6} pc	9.63×10^{-4} pc	9.63×10^{-4} pc
$[m_{\mathrm{BH,min}}, m_{\mathrm{BH,max}}]$	$[5, 50]\, M_\odot$	$[5, 50]\, M_\odot$	$[5, 50]\, M_\odot$
$[q_{\min}, q_{\max}]$	$[0.01, 1]$	$[0.01, 1]$	$[0.01, 1]$
$[a_{0,\min}, a_{0,\max}]$	$[0.1, 100]$ AU	$[0.1, 100]$ AU	$[0.1, 100]$ AU
$[e_{0,\min}, e_{0,\max}]$	$[0.001, 0.99]$	uniform $[0.001, 0.99]$	0.001
M_{SMBH}	$1 \times 10^6 M_\odot$	$1 \times 10^8 M_\odot$	$1 \times 10^8 M_\odot$
$\mathcal{I}_{r,\tilde{M},q,a_0,e_0}$	$(20, 10, 10, 10, 20)$	$(20, 10, 10, 10, 20)$	$(20, 10, 10, 10, 20)$
τ_{avg} [years]	3.12×10^9	1.80×10^7	1.49×10^8
τ_{med} [years]	1.59×10^8	2.60×10^5	1.23×10^8
$\mathcal{R}$ [year^{-1} Gpc^{-3}]	3.9×10^{-2}	0.40	5.68×10^{-6}

$r_{\min}$	9.63×10^{-6} pc	9.63×10^{-4} pc	9.63×10^{-4} pc
$[m_{\mathrm{BH,min}}, m_{\mathrm{BH,max}}]$	$[5, 50]\, M_\odot$	$[5, 50]\, M_\odot$	$[5, 50]\, M_\odot$
$[q_{\min}, q_{\max}]$	$[0.01, 1]$	$[0.01, 1]$	1
$[a_{0,\min}, a_{0,\max}]$	$[0.1, 100]$ AU	uniform $[0.1, 100]$ AU	$[0.1, 100]$ AU
$[e_{0,\min}, e_{0,\max}]$	$[0.001, 0.99]$	$[0.001, 0.99]$	$[0.001, 0.99]$
M_{SMBH}	$1 \times 10^6 M_\odot$	$1 \times 10^8 M_\odot$	$1 \times 10^8 M_\odot$
$\mathcal{I}_{r,\tilde{M},q,a_0,e_0}$	$(20, 10, 10, 10, 20)$	$(20, 10, 10, 10, 20)$	$(20, 10, 10, 10, 20)$
τ_{avg} [years]	3.12×10^9	2.22×10^7	2.31×10^7
τ_{med} [years]	1.59×10^8	4.61×10^5	5.25×10^5
$\mathcal{R}$ [year^{-1} Gpc^{-3}]	3.9×10^{-2}	0.99	0.24

5 Conclusion

6 References

1. *Stacks Project* https://stacks.math.columbia.edu.

2. Thorne, K. S. Multipole expansions of gravitational radiation. *Rev. Mod. Phys.* **52,** 299–339 (2 1980).

3. Peters, P. C. & Mathews, J. Gravitational Radiation from Point Masses in a Keplerian Orbit. *Phys. Rev.* **131,** 435–440 (1 1963).

4. Peters, P. C. Gravitational Radiation and the Motion of Two Point Masses. *Phys. Rev.* **136,** B1224–B1232 (4B 1964).

5. Hansen, R. O. Post-Newtonian Gravitational Radiation from Point Masses in a Hyperbolic Kepler Orbit. *Phys. Rev. D* **5,** 1021–1023 (4 1972).

6. Turner, M. Gravitational radiation from point-masses in unbound orbits - Newtonian results. *The Astrophysical Journal* **216,** 610–619 (Sept. 1977).

7. Junker, W. & Schaefer, G. Binary systems - Higher order gravitational radiation damping and wave emission. *Monthly Notices of the Royal Astronomical Society* **254,** 146–164 (Jan. 1992).

8. De Vittori, L., Jetzer, P. & Klein, A. Gravitational wave energy spectrum of hyperbolic encounters. *Phys. Rev. D* **86,** 044017 (4 2012).

9. García-Bellido, J. & Nesseris, S. Gravitational wave energy emission and detection rates of Primordial Black Hole hyperbolic encounters. *Physics of the Dark Universe* **21,** 61 –69. ISSN: 2212-6864 (2018).

10. Watson, G. N. *A Treatise on the Theory of Bessel Functions* (Cambridge University Press, 1966).

11. Abramowitz, M & Stegun, I. *Handbook of Mathematical Functions* (DOVER PUBN INC, 1965).

12. De Vittori, L., Gopakumar, A., Gupta, A. & Jetzer, P. Gravitational waves from spinning compact binaries in hyperbolic orbits. *Phys. Rev. D* **90,** 124066 (12 2014).

13. Olver, F. W. J. The Asymptotic Expansion of Bessel Functions of Large Order. *Philosophical Transactions of the Royal Society of London. Series A, Mathematical and Physical Sciences* **247,** 328–368. ISSN: 00804614 (1954).

14. Thompson, T. A., Quataert, E. & Murray, N. Radiation Pressure–supported Starburst Disks and Active Galactic Nucleus Fueling. *The Astrophysical Journal* **630,** 167–185 (2005).

15. Kormendy, J. & Ho, L. C. Coevolution (Or Not) of Supermassive Black Holes and Host Galaxies. *Annual Review of Astronomy and Astrophysics* **51,** 511–653 (Aug. 2013).

16. Lubow, P. S. H. & Artymowicz. *Evolutionary Processes in Binary Stars* (ed R. A. M. J. Wijers, . C. A. T. M. B. Davies) (NATO ASIC Proc. 477, 1996).

17. Artymowicz, P. & Lubow, S. H. Dynamics of binary-disk interaction. 1: Resonances and disk gap sizes. *The Astrophysical Journal* **421,** 651–667 (Feb. 1994).

18. Hayasaki, K., Mineshige, S. & Sudou, H. Binary Black Hole Accretion Flows in Merged Galactic Nuclei. *Publications of the Astronomical Society of Japan* **59,** 427–441. ISSN: 0004-6264 (2007).

19. Baruteau, C., Cuadra, J. & Lin, D. N. C. BINARIES MIGRATING IN A GASEOUS DISK: WHERE ARE THE GALACTIC CENTER BINARIES? *The Astrophysical Journal* **726,** 28 (2010).

20. McKernan, B. *et al.* Constraining Stellar-mass Black Hole Mergers in AGN Disks Detectable with LIGO. *The Astrophysical Journal* **866,** 66 (2018).

21. Kroupa, P. The Initial Mass Function of Stars: Evidence for Uniformity in Variable Systems. *Science* **295,** 82–91 (Jan. 2002).

22. Maschberger, T. On the function describing the stellar initial mass function. *Monthly Notices of the Royal Astronomical Society* **429,** 1725–1733. ISSN: 0035-8711 (Dec. 2012).

23. Lauer, T. R. *et al.* The Centers of Early-Type Galaxies with HST.I.An Observational Survey. *The Astrophysical Journal* **110,** 2622 (Dec. 1995).

24. Schödel, R. *et al.* The distribution of stars around the Milky Way´s central black hole - II. Diffuse light from sub-giants and dwarfs. *A&A* **609,** A27 (2018).

25. A. Rasskazov, B. K. The rate of stellar mass black hole scattering in galactic nuclei. *Submitted to the Astrophysical Journal* (2019).

26. Tout, C. A., Hurley, J. R. & Pols, O. R. Evolution of binary stars and the effect of tides on binary populations. *Monthly Notices of the Royal Astronomical Society* **329,** 897–928. ISSN: 0035-8711 (Feb. 2002).

27. Ablimit, I. & Maeda, K. Monte Carlo Population Synthesis on Massive Star Binaries: Astrophysical Implications for Gravitational-wave Sources. *The Astrophysical Journal* **866,** 151 (2018).

28. Maggiore, M. *Gravitational Waves: Volume 1: Theory and Experiments* (Oxford University Press, 2007).

7 Appendix

7.1 Alternative calculation of frequency spectrum

Equation (63) gives the power emitted in the n-th harmonic of an elliptic Keplerian orbit. Here there is similar derivation of the same result which does not explicitly use Parseval's identity. The calculations follows the textbook by Maggiore [28]. Again, we parametrize an elliptic Keplerian orbit in the form

$$x(\beta) = a(\cos u - e), \tag{182}$$
$$y(\beta) = b \sin u. \tag{183}$$

Here a is the semi-major axis and b is the semi-minor axis of the orbit. The eccentric anomaly u is defined by the Kepler equation

$$u - e \sin u = \omega(t - t_0) \equiv \beta, \tag{184}$$

the time t_0 being an integration constant chosen such that $x(-\beta) = x(\beta)$ and $y(\beta) = -y(-\beta)$. The solution of the Kepler equation can be given as a Fourier expansion involving Bessel functions. To see this we make the Fourier series ansatz

$$y(\beta)\frac{e}{b} = u - \beta = e \sin u = \sum_{n=1}^{\infty} a_n \sin(n\beta), \tag{185}$$

where the coefficients are given by

$$a_m = \frac{2}{\pi} \int_0^\pi d\beta\, (u - \beta) \sin(m\beta). \tag{186}$$

We now compute

$$
\begin{aligned}
a_m &= -\frac{2e}{\pi m} \int_0^\pi d\beta\, \sin u\, \frac{d}{d\beta} \cos(m\beta) \\
&= \frac{2e}{\pi m} \int_0^\pi du\, \frac{d \sin u}{du}\, \cos(m\beta) \\
&= \frac{2e}{\pi m} \int_0^\pi du\, \cos u\, \cos(mu - me \sin u) \\
&= \frac{e}{m} \int_0^\pi \frac{du}{\pi}\, \left[\cos(u(m-1) - me \sin u) + \cos(u(m+1) - me \sin u)\right].
\end{aligned}
$$

By using the following integral representation of the Bessel functions of the first kind

$$J_n(z) = \int_0^\pi \frac{du}{\pi} \cos(nu - z \sin u), \tag{187}$$

we arrive at

$$a_m = \frac{e}{m} \left[J_{m-1}(me) + J_{m+1}(me)\right]. \tag{188}$$

Using the recurrence formula

$$J_{n-1}(z) + J_{n+1}(z) = \frac{2n}{z} J_n(z), \tag{189}$$

this result can be rewritten as

$$a_m = \frac{2}{m} J_m(me). \tag{190}$$

Similarly we write $\frac{x(\beta)}{a} = \cos u - e = b_0 + \sum_{n=1}^{\infty} b_n \cos(n\beta)$ and find for the corresponding expansion coefficients

$$b_0 = -\frac{3}{2}e, \tag{191}$$

$$b_m = \frac{1}{m}[J_{m-1}(z) - J_{m+1}(z)] = \frac{2}{m} J_m'(me); \tag{192}$$

the prime denotes the derivative with respect to the argument. Next we compute the Fourier expansion of $x^2(\beta)$, $y^2(\beta)$ and $x(\beta)y(\beta)$. We can again write

$$y^2(\beta) = A_0 + \sum_{n=1}^{\infty} A_n \cos(n\beta), \tag{193}$$

$$x^2(\beta) = B_0 + \sum_{n=1}^{\infty} B_n \cos(n\beta), \tag{194}$$

$$y(\beta)x(\beta) = \sum_{n=1}^{\infty} C_n \sin(n\beta), \tag{195}$$

together with

$$A_m = \frac{2}{\pi} \int_0^{\pi} d\beta \, y^2(\beta) \cos(m\beta), \tag{196}$$

$$B_m = \frac{2}{\pi} \int_0^{\pi} d\beta \, x^2(\beta) \cos(m\beta), \tag{197}$$

$$C_m = \frac{2}{\pi} \int_0^{\pi} d\beta \, x(\beta)y(\beta) \sin(m\beta). \tag{198}$$

Similar to the calculation of a_n we obtain

$$A_m = \frac{b^2}{m} [J_{m+2}(me) - J_{m-2}(me)],$$

$$B_m = \frac{a^2}{m} [J_{m-2}(me) - J_{m+2}(me) - 2e(J_{m-1}(me) - J_{m+1}(me))],$$

$$C_m = \frac{ba}{m} [J_{m+2}(me) + J_{m-2}(me) - e(J_{m+1}(me) + J_{m-1}(me))],$$

along with $A_0 = \frac{1}{2}$ and $B_0 = \frac{1+4e^2}{2}$. By the use of the recurrence relations (189) and (192) the above relations can be expressed entirely in terms of J_m and its derivative. We obtain

$$A_m = \frac{4b^2}{me} \left[\frac{1}{me} J_m(me) - J_m'(me) \right],$$

$$B_m = \frac{4a^2}{m} \left[\left(\frac{1}{e} - e \right) J_m'(me) - \frac{1}{me^2} J_m(me) \right], \tag{199}$$

$$C_m = \frac{4ba}{m} \left[\left(\frac{1}{e^2} - 1 \right) J_m(me) - \frac{1}{me} J_m'(me) \right].$$

50

With the above we are able to expand the second mass moment (21) as

$$\mathcal{G} = \mu \sum_{n=0}^{\infty} \begin{bmatrix} B_n \cos(n\beta) & C_n \sin(n\beta) & 0 \\ C_n \sin(n\beta) & A_n \cos(n\beta) & 0 \\ 0 & 0 & 0 \end{bmatrix} \equiv \sum_{n=0}^{\infty} \mathcal{G}^{(n)}. \tag{200}$$

The emitted power in the quadrupole approximation is obtained from the formulae (16) and (29)

$$P = \frac{8\pi}{75} \sum_{m=-2}^{2} \left\langle \left| {}^{(3)}\mathcal{G}_{a_1 a_2} \left(\mathcal{Y}_{a_1 a_2}^{2m} \right)^* \right|^2 \right\rangle. \tag{201}$$

Since $\langle \cos(n\beta) \cos(m\beta) \rangle = \langle \sin(n\beta) \sin(m\beta) \rangle = \frac{1}{2}\delta_{mn}$, different harmonics don't contribute in the power spectrum. Hence we can set $P = \sum_{n=1}^{\infty} P_n$, where the power radiated in the n-th harmonics is

$$P_n = \frac{8\pi}{75} \sum_{m=-2}^{2} \left\langle \left| {}^{(3)}\mathcal{G}_{a_1 a_2}^{(n)} \left(\mathcal{Y}_{a_1 a_2}^{2m} \right)^* \right|^2 \right\rangle, \tag{202}$$

together with

$$^{(3)}\mathcal{G}^{(n)} = \mu(\omega n)^3 \begin{bmatrix} B_n \sin(n\beta) & -C_n \cos(n\beta) & 0 \\ -C_n \cos(n\beta) & A_n \sin(n\beta) & 0 \\ 0 & 0 & 0 \end{bmatrix}. \tag{203}$$

Using the above formulae gives the power in the n-th harmonic as

$$P_n = \frac{1}{15} \mu^2 (\omega n)^6 \left(A_n^2 + B_n^2 + 3C_n^2 - A_n B_n \right). \tag{204}$$

We can now insert the explicit form of the coefficients (199) and after rearranging terms we find that P_n is equal to (63).

7.2 Discretized distributions of binary parameters

Here we give the formulae for the number $N_{x,i}$ of BBHs inside a bin $i \in \mathcal{I}_x$ of the binary parameter $x = \{\tilde{M}, q, e_0, a_0\}$ and the average value x_i of the quantity x within bin i.

Primary mass The number of primary BHs within the mass bin $[m_{\mathrm{BH,min}} + i\Delta M, m_{\mathrm{BH,min}} + (i+1)\Delta M]$, where $\Delta M = (m_{\mathrm{BH,max}} - m_{\mathrm{BH,min}})/|\mathcal{I}_{\tilde{M}}|$ and $i \in \mathcal{I}_{\tilde{M}}$, is obtained by integrating equation (175) with respect to m

$$
N_{\tilde{M},i} = \frac{f_b f_d}{2} \frac{4\pi k \rho_0 \xi_0}{1.35} \left[(m_{\mathrm{BH,min}} + i\Delta M)^{-1.35} - (m_{\mathrm{BH,min}} + (i+1)\Delta M)^{-1.35} \right]
$$

$$
\times \begin{cases} \frac{1}{3-\gamma} r_b^\gamma \left[(r_{\min} + (j+1)\Delta r)^{3-\gamma} - (r_{\min} + j\Delta r)^{3-\gamma} \right] & \text{if } r_{\min} + (j+1)\Delta r \le r_b \\ \frac{1}{3-\beta} r_b^3 \left[\left(\frac{r_{\min} + (j+1)\Delta r}{r_b} \right)^{3-\beta} - \left(\frac{r_{\min} + j\Delta r}{r_b} \right)^{3-\beta} \right] & \text{if } r_{\min} + j\Delta r > r_b \end{cases}
$$
(205)

The average mass within this mass bin is

$$
\tilde{M}_i = \frac{1.35}{0.35} \frac{\left[(m_{\mathrm{BH,min}} + i\Delta M)^{-0.35} - (m_{\mathrm{BH,min}} + (i+1)\Delta M)^{-0.35} \right]}{\left[(m_{\mathrm{BH,min}} + i\Delta M)^{-1.35} - (m_{\mathrm{BH,min}} + (i+1)\Delta M)^{-1.35} \right]}.
$$
(206)

Mass ratio Using (176), the number of BBH within the mass ratio bin $[q_{\min} + i\Delta q, q_{\min} + (i+1)\Delta q]$, where $\Delta q = (q_{\max} - q_{\min})/|\mathcal{I}_q|$ and $i \in \mathcal{I}_q$, is

$$
N_{q,i} = \vartheta_0 \Delta q.
$$
(207)

The average mass ratio within this mass ratio bin is

$$
q_i = (i + 0.5)\Delta q + q_{\min}.
$$
(208)

Orbital separation The number of BBH within the orbital separation bin $[a_{0,\min} + i\Delta a, a_{0,\min} + (i+1)\Delta a]$, where $\Delta a = (a_{0,\max} - a_{0,\min})/|\mathcal{I}_{a_0}|$ and $i \in \mathcal{I}_{a_0}$, is from the distribution (177)

$$
N_{a_0,i} = \chi_0 \log \left(\frac{a_{0,\min} + (i+1)\Delta a}{a_{0,\min} + i\Delta a} \right).
$$
(209)

The average a_0 within this bin is

$$
a_{0_i} = \frac{\Delta a}{\log \left(\frac{a_{0,\min} + (i+1)\Delta a}{a_{0,\min} + i\Delta a} \right)}.
$$
(210)

Orbital eccentricity The number of BBH within the eccentricity bin $[e_{0,\min} + i\Delta e_0, e_{0,\min} + (i+1)\Delta e_0]$, where $\Delta e_0 = (e_{0,\max} - e_{0,\min})/|\mathcal{I}_{e_0}|$ and $i \in \mathcal{I}_{e_0}$, is using the distribution (178)

$$
N_{e_0,i} = \varsigma_0 (i + 0.5) (\Delta e_0)^2 + \varsigma_0 e_{0,\min} \Delta e.
$$
(211)

The average e_0 within this bin is

$$
e_{0_i} = \frac{6e_{0,\min}^2 + 6e_{0,\min}(2i\Delta e + \Delta e) + 2\Delta e^2 (3i^2 + 3i + 1)}{3(2e_{0,\min} + 2i\Delta e + \Delta e)}.
$$
(212)